

Quantum Dynamics and Statistical Mechanics of Endohedral Water

by

Spencer Yim

A thesis
presented to the University of Waterloo
in fulfillment of the
thesis requirement for the degree of
Master of Science
in
Chemistry

Waterloo, Ontario, Canada, 2016

© Spencer Yim 2016

Author's Declaration

I hereby declare that I am the sole author of this thesis. This is a true copy of the thesis, including any required final revisions, as accepted by my examiners.

I understand that my thesis may be made electronically available to the public.

Abstract

Since first being synthesized in 2011, $\text{H}_2\text{O}@\text{C}_{60}$ has attracted much attention in the literature. Many interesting quantum phenomena are associated with this system, including ortho-para conversion, rotational ground state splitting, and long-range dipole correlations. The work presented here covers the theory required to model such a system as well as detailing two projects that were undertaken in order to develop tools to study $\text{H}_2\text{O}@\text{C}_{60}$.

Path integral molecular dynamics simulations were utilized to gain an understanding of the thermodynamic properties such as position and orientation densities, and imaginary-time autocorrelation functions (ITACFs) were investigated and compared to those of a free water molecule.

In order to gain access to energy levels directly, code was also developed in order to diagonalize the Hamiltonian for the system and obtain the exact energy levels variationally. The code that was written for this purpose is very general and can easily be applied to a wide number of similar systems, including different guest/host molecules.

Acknowledgements

I would first and foremost like to thank my supervisor Pierre-Nicholas Roy for his infinite patience, enthusiasm, and wisdom throughout the last couple of years. Next, I want to take the opportunity to thank the rest of my Advisory Committee, including Professor Marcel Nooijen and Professor Scott Hopkins.

Additionally, I would like to extend a big thank you to the rest of the Theoretical Chemistry group here at the University of Waterloo especially: Dmitri, Lindsay, Matt, Kevin, Neil, and Max. You're all the best.

Contents

List of Figures	vii
1 Introduction	1
1.1 Water Inside of a Buckyball	2
2 Background Theory	6
2.1 Statistical Mechanics	8
2.1.1 Thermal Wavefunction	9
2.1.2 Expectation Values	10
2.1.3 Autocorrelation Functions	11
2.2 Rotational States of Water	13
2.2.1 Contribution to Thermodynamic Energy	16
2.3 Exact Imaginary Time Orientation Autocorrelation Functions	16
3 Path Integral Molecular Dynamics	22
3.1 Path Integral Formulation of the Partition Function	22
3.2 Thermodynamic Estimators	26
3.3 Parameter Optimization	27
3.3.1 Centroid Friction Coefficient	27
3.3.2 Timestep	29
3.3.3 Energy vs. τ Convergence	30
3.4 Density Distributions	32

3.4.1	Center-of-Mass Position Distribution	32
3.4.2	Orientation Distributions	35
3.5	Imaginary Time Autocorrelation Functions	41
4	Exact Diagonalization	45
4.1	Hamiltonian – Setting the Stage	45
4.2	Calculating the Potential	46
4.3	Choosing a Basis	47
4.3.1	$\langle JKM $	48
4.3.2	$\langle klm $	48
4.4	Matrix Elements	49
4.5	Code Testing and Preliminary Results	50
4.6	Outlook	53
5	Conclusion	54
5.1	Future Work	55
	References	56
	Appendix A Exact ITACF using Spherical Coordinates	59
	Appendix B Classical Motion of a QHO using Thermal Wavefunction	71
	Appendix C Useful Snippets of Code	76
C.1	Little-D Function	76
C.2	Rotational Hamiltonian Setup	77
C.3	Indexing and Basis Size Formulas	77

List of Figures

1	Low Lying Rotational Energy Levels of H ₂ O	3
2	PES for H ₂ O@C ₆₀	7
3	Minimum of PES for H ₂ O@C ₆₀ vs COM Position	8
4	Water-fixed frame Cartesian Axes	14
5	Rotational Contribution to Thermodynamic Energy	16
6	Exact ITACF of H ₂ O@C ₆₀ , T=4K	20
7	Exact ITACF of H ₂ O@C ₆₀ , T=12K	21
8	Exact ITACF of H ₂ O@C ₆₀ , T=55k	21
9	Path Integral Representation of Water	25
10	Auto-correlation Functions for Oxygen and Water Dipole - 0 ps ⁻¹	28
11	Auto-correlation Functions for Oxygen and Water Dipole - 1 ps ⁻¹	29
12	Auto-correlation Functions for Oxygen and Water Dipole - 100 ps ⁻¹	29
13	Timestep Convergence	30
14	Energy Convergence at 4K	31
15	Energy Convergence at 55K	31
16	Center-of-Mass Density at 4K	32
17	Center-of-Mass Density at 360K	33
18	Center-of-Mass x-Density	33
19	Center-of-Mass y-Density	34
20	Center-of-Mass z-Density	34

21	Principal Axis ϕ Distributions at 4 K	36
22	Principal Axis ϕ Distributions at 360 K	36
23	A-axis ϕ Distributions	37
24	B-axis ϕ Distributions	37
25	C-axis ϕ Distributions	38
26	Principal Axis $\cos(\theta)$ Distributions at 4K	38
27	Principal Axis $\cos(\theta)$ Distributions at 360K	39
28	A-axis $\cos(\theta)$ Distributions	39
29	B-axis $\cos(\theta)$ Distributions	40
30	C-axis $\cos(\theta)$ Distributions	40
31	PIMD Orientational ITACF - 4K	41
32	PIMD Orientational ITACF - 12K	42
33	PIMD Orientational ITACF - 360K	42
34	PIMD Orientational ITACF - A Axis	43
35	PIMD Orientational ITACF - B Axis	43
36	PIMD Orientational ITACF - C Axis	44

Chapter 1

Introduction

Molecules have been found to exhibit interesting quantum properties within various confining geometries.¹⁻⁴ These quantum properties can include effects such as spatial anisotropy induced rotational level splitting, and “quantum rattling”, which manifests itself in the translational movement of the molecule. There are a number of systems that may fall under the category of “nano-cavities”, but specific examples are: molecular hydrogen in a clathrate cage, water in rare gas matrices, and endohedral fullerene complexes.

The work presented focuses on a water molecule that has been encapsulated within a buckyball ($\text{H}_2\text{O}@C_{60}$), and is organized into four main sections. First, a formal introduction to the system is provided, involving a very brief review of experimental results highlighting the interesting quantum phenomena that arises. Secondly, relevant background theory required for a thorough understanding of the works is covered. The third and fourth sections detail the results and discussion of two projects undertaken in order to investigate the system, path integral molecular dynamics simulations and exact diagonalization calculations.

1.1 Water Inside of a Buckyball

The endohedral water fullerene complex was first synthesized in 2011⁵ in a molecular surgery approach that has since been improved on.⁶ The result was a very exciting system rich in quantum phenomena that may have eventual applications in many fields, spurring interest and subsequently numerous studies.^{7–20}

Some of the results from these experiments will be briefly discussed below, as they provide us with motivation for studying such a system.

Inelastic Neutron Scattering

Very briefly, inelastic neutron scattering is a technique that is dependent on nuclear spin interactions with the sample. Similar to molecular hydrogen, water molecules may be found in either a *para*-state, or an *ortho*-state. *Para* water corresponds to the molecule having a total nuclear spin of 0, whereas *ortho* water has a total nuclear spin 1, which is based on the spins of the hydrogen atoms. The INS technique may actually drive transitions between these spin-isomers of H_2O , so INS peaks appear that correspond to *ortho*–*para* transitions. Likewise, since *ortho* water has spin 1, *ortho*–*ortho* transitions may also be seen.

Figure 1 shows the low lying rotational energy levels of a free water molecule, and will be imperative to understanding much of the discussion in this work. The energy level diagram is divided into the *para* states and the *ortho* states. *Para* states correspond to a quantum number K being even in the symmetric top basis $|JKM\rangle$, and *ortho* states odd.

In an experiment using INS conducted by Turro et al.,⁹ they found evidence of a splitting in the ground state of the *ortho* level. The data obtained seemed to indicate that the triply degenerate level split by 0.6 meV into a doubly and singly degenerate level.

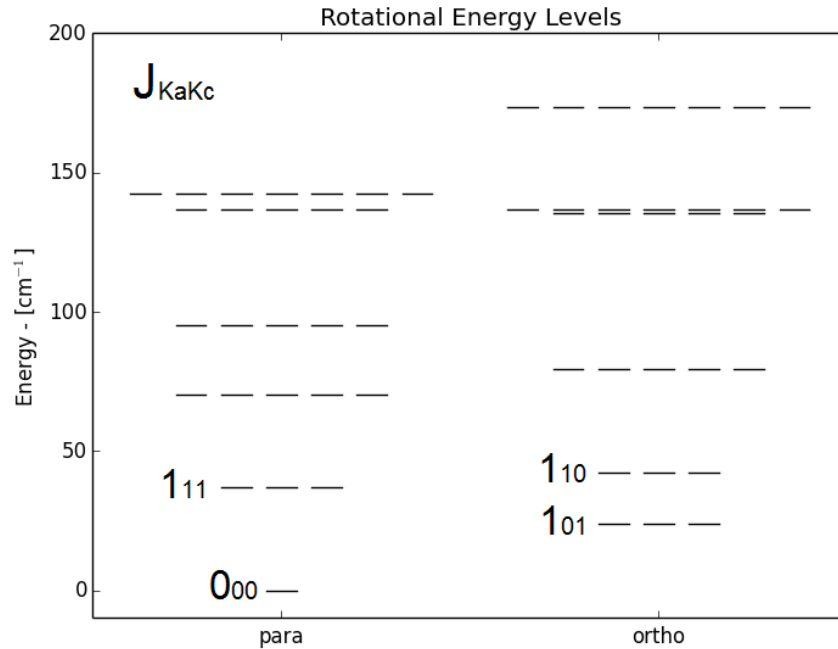


Figure 1: Low Lying Rotational Energy Levels of H₂O

Far-Infrared Spectroscopy

The infrared spectrum is typically divided into three categories: near, mid, and far-infrared. The far-infrared region ranges from about 400 cm^{-1} – 10 cm^{-1} . At such a low energy, the rotational states of the system under study may be directly probed. Since this type of spectroscopy cannot flip nuclear spin, *ortho-para* transitions are forbidden and the peaks that are identified are strictly *ortho-ortho* and *para-para* transitions. The FIR spectra of this system was obtained by Turro et al.⁹ at three different times relative to the time the sample was prepared: immediately after the sample was prepared, 13 hours after preparation, and once more 48 hours after preparation. *ortho-para* conversion was observed through the fact that the relative intensity of the *para* transitions and the *ortho* transitions changed over the duration of the data collection.

Nuclear Magnetic Resonance

Nuclear magnetic resonance is a very powerful technique that has been used in a number of studies regarding $\text{H}_2\text{O}@\text{C}_{60}$.^{9,10} It has been used in order to study the *ortho-para* water conversion. The kinetics can be observed by measuring the decreasing *ortho* signal (*para* water is not NMR active due to the spin being 0). It was determined that the conversion followed second-order kinetics which is consistent with bimolecular models for the spin conversion, although the exact mechanism for such a process remains unclear.

In another NMR study, they were able to observe level splitting in the *ortho* ground state, as well as an anisotropic interaction that disappears at higher frequencies of the Magic Angle Spinning NMR (MAS-NMR) technique.

X-ray Structure Analysis

The crystal structure of $\text{H}_2\text{O}@\text{C}_{60}$ was determined using X-ray diffraction.¹⁹ It was found that, much like empty C_{60} , the material took on a face-centered cubic (fcc) structure at room temperature, and goes through structural transformation to simple cubic (sc) at around 260 K, also like empty C_{60} . The lattice constant for the $\text{H}_2\text{O}@\text{C}_{60}$ is larger than C_{60} in the fcc conformation, but they are fairly equal in the sc phase.

Dielectric Permittivity Measurements

The dielectric permittivities of both $\text{H}_2\text{O}@\text{C}_{60}$ and C_{60} were measured and plotted against temperature.¹⁹ The behaviour of the endohedral fullerene is quite different from that of pure buckyballs as the permittivity increases with decreasing temperature following the Curie-Weiss law,²¹ whereas the empty fullerene remains relatively constant. Both materials exhibit a small jump in permittivity at about the same temperature that they transform from fcc to sc. This increase in dielectric permittivity indicates longer range correlations between the dipole moments of the water molecules.

These experiments highlight the interesting quantum phenomena associated with the

endohedral water system, namely: *ortho-para* spin conversion, rotational level-splitting, and long-range dipole correlations. The rest of this work relates to the theory involved with modeling such a system, and the quantum simulations and calculations that were developed.

The remainder of this thesis is organized as follows: Chapter 2 contains a description of the background theory required for a thorough understanding of the system, Chapter 3 contains a description of the path integral simulations that were run on this system, Chapter 4 contains a description of the exact diagonalization code that was developed in order to obtain exact energy values, and conclusions and future directions are presented in Chapter 5.

Chapter 2

Background Theory

In order to tractably investigate the quantum dynamics of $\text{H}_2\text{O}@C_{60}$, we must work within the framework of the Born-Oppenheimer approximation. That is to say, the nuclear motion of the atoms within the water molecule are much slower compared to the fast movement of the electrons and can be uncoupled from each other. Thus for a given set of nuclear coordinates, the electronic problem may be solved in order to give a potential energy. When done at many different nuclear positions, we may define a potential energy surface (PES) for the system to be used in determining the nuclear dynamics.

The potential energy surface that will be used in this work is defined via a regular 6-12 Lennard-Jones pair-interaction potential which has the form:

$$V_{LJ} = 4\epsilon \left[\left(\frac{\sigma}{r} \right)^{12} - \left(\frac{\sigma}{r} \right)^6 \right] \quad (2.1)$$

ϵ and σ are the parameters describing the interaction between two entities. In this work, ϵ and σ are taken from a study published in 2013 by Farimani et al.¹⁴ in which the rotation of water inside a buckyball was studied using classical molecular dynamics (MD) simulations. The parameters were obtained through curve fitting a DFT-SAPT (density functional theory-symmetry adapted perturbation theory) ab initio graphene-water interaction, and were reported as:

$$\begin{aligned}\sigma_{C-OW} &= 3.372\text{\AA} \\ \epsilon_{C-OW} &= 0.1309 \frac{\text{kcal}}{\text{mol}} \\ \sigma_{H-OW} &= 2.640\text{\AA} \\ \epsilon_{H-OW} &= 0.0256 \frac{\text{kcal}}{\text{mol}}\end{aligned}$$

The PES obtained for this model of interaction is depicted below, where the potential is scanned with increasing r along the three principal axis with a fixed orientation.

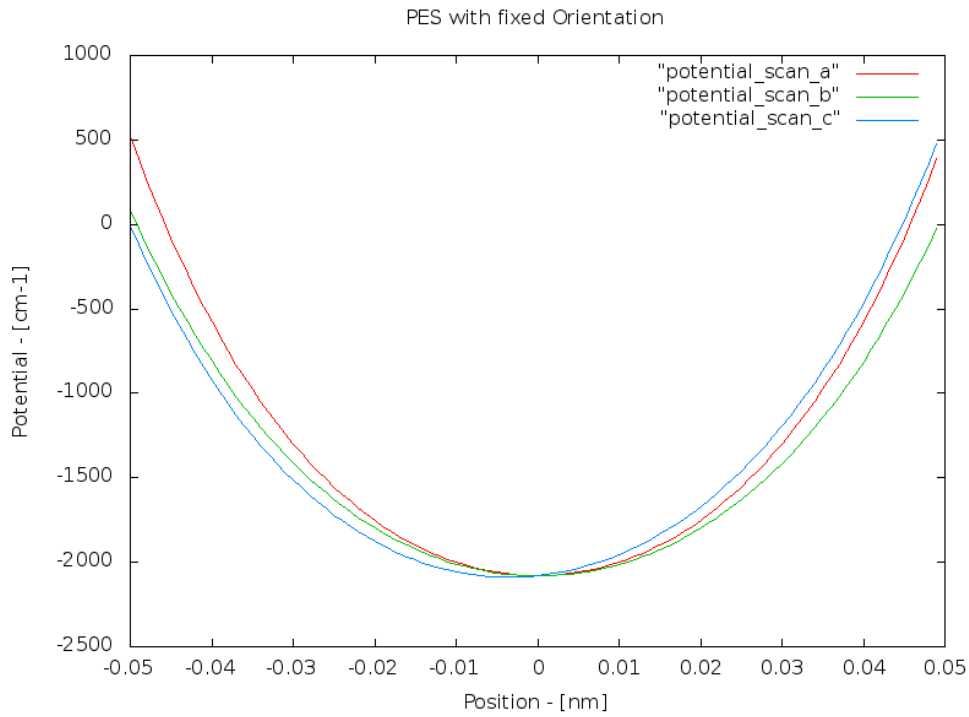


Figure 2: PES for $\text{H}_2\text{O}@C_{60}$ along Principal Axes of Inertia

If instead of fixing the molecular orientation and scanning along each principal axis, but we instead allow the water to find the minimum orientation for a fixed center-of-mass position, we find a symmetric double-well with an extremely small barrier height.

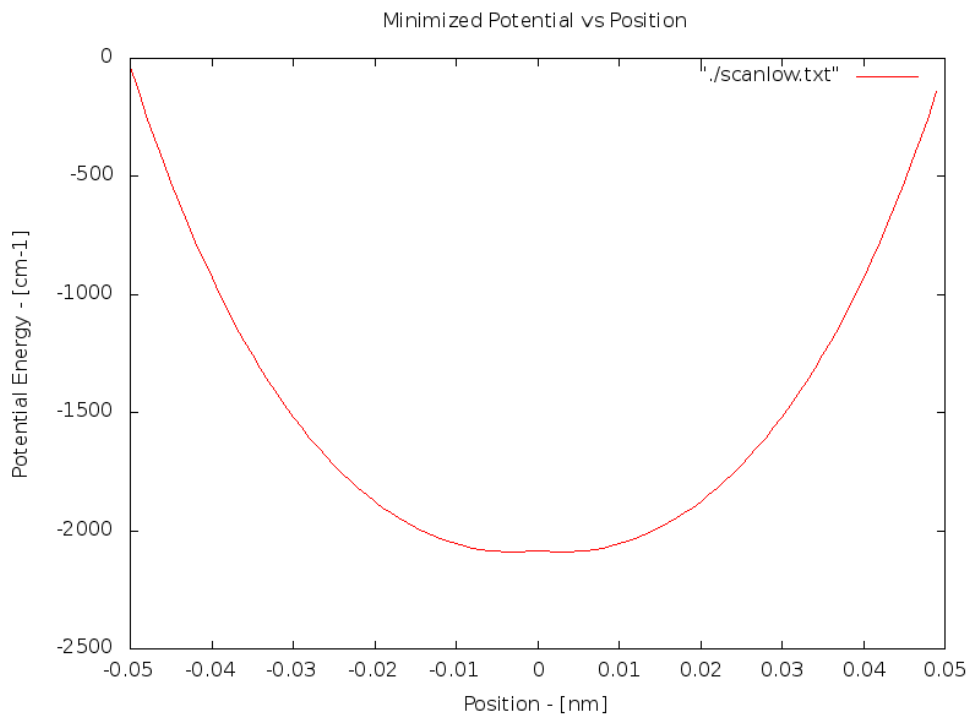


Figure 3: Minimum of PES for $\text{H}_2\text{O}@C_{60}$ vs COM Position

2.1 Statistical Mechanics

Statistical mechanics is extremely important when trying to calculate real properties of systems with quantum precision. It provides us with a tool to determine macroscale properties of materials that arise due to the quantum properties and interactions of individual molecules themselves.

Central to the development of statistical mechanics is the canonical partition function:

$$Z = \text{Tr} [\hat{\rho}] \tag{2.2}$$

where Tr represents the trace, and ρ is defined as $e^{-\beta\hat{H}}$, where $\beta = \frac{1}{k_B T}$, k_B is Boltzmann's constant, T is the temperature and \hat{H} is the Hamiltonian describing the system of interest. If the trace is performed in the energy eigen basis:

$$Z = \sum_n e^{-\beta E_n} \quad (2.3)$$

If one is interested in average thermodynamic properties, one can calculate:

$$\langle \hat{O} \rangle = \frac{\text{Tr} [\hat{\rho} \hat{O}]}{\text{Tr} [\hat{\rho}]} \quad (2.4)$$

where \hat{O} is some operator of interest.

2.1.1 Thermal Wavefunction

It may be intuitive to construct a thermal wavefunction in order to calculate thermodynamic properties. If a system is at thermal equilibrium, then instead of writing a statistical mixture, we may assume that the system is in a superposition of eigenstates. The amplitude of each state is postulated to be equivalent to the Boltzmann factor of that state. Thus for a given system at some temperature T , the wavefunction at thermal equilibrium can be written as:

$$|\psi(\beta)\rangle \quad (2.5)$$

Expanding into the energy basis, we find:

$$\begin{aligned} |\psi(\beta)\rangle &= \sum_n |n\rangle \langle n|\psi(\beta)\rangle \\ &= \frac{1}{\sqrt{Z}} \sum_n e^{-\frac{\beta E_n}{2}} e^{i\theta_n} |n\rangle \end{aligned}$$

where θ_n is a random phase associated with the n-th eigenstate and is attributed to the random thermalization process.

A wavefunction defined in this way will have the same time-averaged properties as if we had created an ensemble that existed as a statistical mixture of eigenstates. This is shown in the next subsections.

2.1.2 Expectation Values

Being able to calculate expectation values for a system is important. The formulation for finite temperature expectation values is given using the 'thermal wavefunctions' introduced previously. Beginning with a time-dependent expectation value, we may obtain the canonical expectation value after averaging over *all* time.

$$\langle \psi | \hat{O}(t) | \psi \rangle \tag{2.6}$$

where $\hat{O}(t)$ represents the time dependence of some operator \hat{O} and can be explicitly written as:

$$\hat{O}(t) = e^{\frac{i\hat{H}t}{\hbar}} \hat{O} e^{-\frac{i\hat{H}t}{\hbar}}$$

By projecting the wavefunctions into the energy basis, we obtain:

$$\sum_n \sum_m \langle \psi | n \rangle \langle n | e^{\frac{i\hat{H}t}{\hbar}} \hat{O} e^{-\frac{i\hat{H}t}{\hbar}} | m \rangle \langle m | \psi \rangle$$

and, using the proposed overlap of the wavefunction with the energy basis at some

finite temperature T we find that:

$$\frac{1}{Z} \sum_n \sum_m e^{-\frac{\beta(E_n+E_m)}{2}} e^{i(\theta_n-\theta_m)} e^{\frac{i(E_n-E_m)t}{\hbar}} \langle n | \hat{O} | m \rangle \quad (2.7)$$

We recognize this expression as the most general working form of the time dependent expectation value of some operator \hat{O} .

In order to recover canonical expectation values, we must average the time dependent expectation value over all possible times, meaning that we will perform a time integral from negative infinity to positive infinity. Since the only term in the above formula that is actually dependent on time is $e^{\frac{i(E_n-E_m)t}{\hbar}}$, the integral can be computed immediately.

$$\frac{1}{2\pi} \int_{-\infty}^{+\infty} e^{\frac{i(E_n-E_m)t}{\hbar}} dt = \delta_{nm}$$

This has the effect of setting m equal to n , which results in:

$$\frac{1}{Z} \sum_n e^{-\beta E_n} \langle n | \hat{O} | n \rangle \quad (2.8)$$

2.1.3 Autocorrelation Functions

Autocorrelation functions provide us with an extremely useful tool to investigate signals. More precisely, the autocorrelation function of a signal tells us how that particular signal changes (usually over time) with respect to some 'lag parameter'.

The exact imaginary time autocorrelation function for operator \hat{O} in terms of the thermal wavefunction defined previously is:

$$\langle \psi | \hat{O}(t) \cdot \hat{O}(t + i\tau) | \psi \rangle \quad (2.9)$$

This is the expectation value between the inner product of the operator \hat{O} at some t with the operator at time t with an imaginary timelag ' $i\tau$ ' added to it. We may proceed to

evaluate this in a similar manner as the expectation value of an operator by first expanding the bra and ket in the energy basis to give us:

$$\begin{aligned}
& \sum_n \sum_m \langle \psi | n \rangle \langle n | e^{\frac{i\hat{H}t}{\hbar}} \hat{O} e^{-\frac{i\hat{H}t}{\hbar}} e^{\frac{i\hat{H}(t+i\tau)}{\hbar}} \hat{O} e^{-\frac{i\hat{H}(t+i\tau)}{\hbar}} | m \rangle \langle m | \psi \rangle \\
& \frac{1}{Z} \sum_n \sum_m e^{-\frac{\beta E_n}{2}} e^{i\theta_n} \langle n | e^{\frac{i\hat{H}t}{\hbar}} \hat{O} e^{-\frac{i\hat{H}\tau}{\hbar}} \hat{O} e^{-\frac{i\hat{H}(t+i\tau)}{\hbar}} | m \rangle e^{-\frac{\beta E_m}{2}} e^{-i\theta_m} \\
& \frac{1}{Z} \sum_n \sum_m e^{-\frac{\beta(E_n+E_m)}{2}} e^{i(\theta_n-\theta_m)} e^{\frac{i(E_n-E_m)t}{\hbar}} e^{\frac{E_m\tau}{\hbar}} \langle n | \hat{O} e^{-\frac{i\hat{H}\tau}{\hbar}} \hat{O} | m \rangle \\
& \frac{1}{Z} \sum_n \sum_m \sum_\gamma e^{-\frac{\beta(E_n+E_m)}{2}} e^{i(\theta_n-\theta_m)} e^{\frac{i(E_n-E_m)t}{\hbar}} e^{\frac{E_m\tau}{\hbar}} \langle n | \hat{O} | \gamma \rangle \langle \gamma | e^{-\frac{i\hat{H}\tau}{\hbar}} \hat{O} | m \rangle \\
& \frac{1}{Z} \sum_n \sum_m \sum_\gamma e^{-\frac{\beta(E_n+E_m)}{2}} e^{i(\theta_n-\theta_m)} e^{\frac{i(E_n-E_m)t}{\hbar}} e^{\frac{\tau(E_m-E_n)}{\hbar}} \langle n | \hat{O} | \gamma \rangle \langle \gamma | \hat{O} | m \rangle \tag{2.10}
\end{aligned}$$

Here we have found the most general form of the imaginary time autocorrelation for the thermal wavefunction, which may be completely meaningless. In order to recover the familiar form of the autocorrelation function we must perform an average over all time, with the same result as above. Once again, the only part of the expression that is dependent on time is $e^{\frac{i(E_n-E_m)t}{\hbar}}$, and we recognize this as a kronecker delta which we recognize as a dirac delta function upon integration. This causes the n and m to become equal, thus only diagonal terms survive and the off-diagonal terms are killed. Finally, we obtain:

$$\frac{1}{Z} \sum_n \sum_\gamma e^{-\beta E_n} e^{\frac{\tau(E_n-E_n)}{\hbar}} \langle n | \hat{O} | \gamma \rangle \langle \gamma | \hat{O} | n \rangle \tag{2.11}$$

$$\frac{1}{Z} \sum_n \sum_\gamma e^{-\beta E_n} e^{\frac{\tau(E_n - E_\gamma)}{\hbar}} \left| \langle n | \hat{O} | \gamma \rangle \right|^2 \quad (2.12)$$

2.2 Rotational States of Water

In order to determine the eigenfunctions of the rotational Hamiltonian for water, we must solve the problem in the symmetric top basis. A brief overview of this process is given following the development of Zare.²²

We may begin by acknowledging the rotational Hamiltonian:

$$\hat{H}_{rot} = AJ_a^2 + BJ_b^2 + CJ_c^2 \quad (2.13)$$

A, B, C are the rotational constants of the molecule and are subsequently defined as:

$$A = \frac{\hbar}{4\pi I_a} \quad (2.14)$$

$$B = \frac{\hbar}{4\pi I_b} \quad (2.15)$$

$$C = \frac{\hbar}{4\pi I_c} \quad (2.16)$$

I_a , I_b and I_c are the three principal moments of inertia (resulting from diagonalization of the moment of inertia tensor). For water, which is an asymmetric top, convention dictates that $I_a < I_b < I_c$, or equivalently $A > B > C$. Also by convention, the z-axis of the molecule in the molecular fixed frame is defined as equivalent to the C_2 axis and the x-axis is parallel to the H-H direction, thus we make the following association with the rotational constants and the coordinate axis:

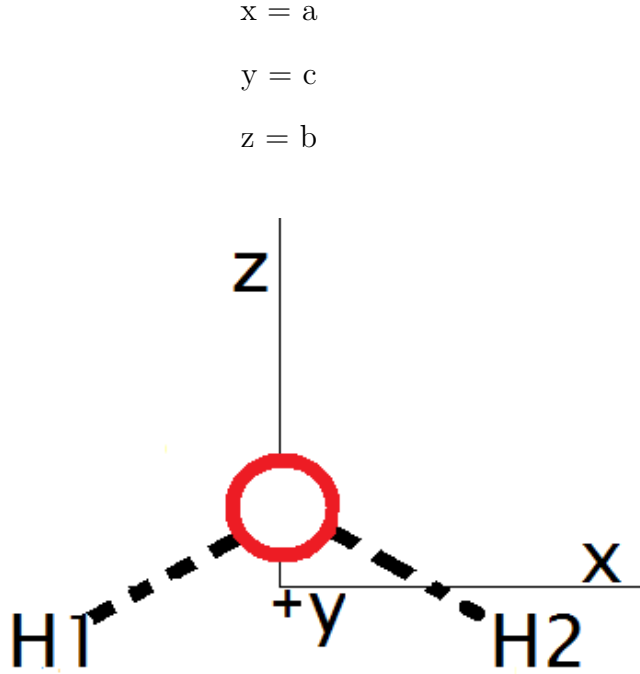


Figure 4: Water-fixed frame Cartesian Axes Diagram

The matrix elements of the angular momentum operators in the symmetric top basis are given now. For the diagonal elements:

$$\langle JKM | J_x^2 | JKM \rangle = \langle JKM | J_y^2 | JKM \rangle = \frac{1}{2} [J(J+1) - K^2] \quad (2.17)$$

$$\langle JKM | J_z^2 | JKM \rangle = K^2 \quad (2.18)$$

and for the off-diagonal elements of the angular momentum operators in the JKM basis:

$$\begin{aligned} \langle JKM | J_x^2 | J[K \pm 2]M \rangle &= -\langle JKM | J_y^2 | J[K \pm 2]M \rangle \\ &= \frac{1}{4} [J(J+1) - K(K \pm 1)]^{\frac{1}{2}} [J(J+1) - (K \pm 1)(K \pm 2)]^{\frac{1}{2}} \end{aligned} \quad (2.19)$$

Now, using the convention of relating the inertial axis to cartesian axis in the molecular frame mentioned above, we may write the Hamiltonian as:

$$\langle JKM | \hat{H}_{rot} | JKM \rangle = \frac{(A+C)}{2} [J(J+1) - K^2] + BK^2 \quad (2.20)$$

$$\begin{aligned} \langle JKM | \hat{H}_{rot} | J[K \pm 2]M \rangle = & \frac{(A-C)}{4} [J(J+1) - K(K \pm 1)]^{\frac{1}{2}} \times \\ & [J(J+1) - (K \pm 1)(K \pm 2)]^{\frac{1}{2}} \end{aligned} \quad (2.21)$$

The Hamiltonian in the JKM basis is diagonal in J and M, thus needs only be solved in K blocks which have a size $(2J+1) \times (2J+1)$ for each J level, with each state being $(2J+1)$ degenerate corresponding to M:

$$M = -J, -J+1, \dots, 0, \dots, +J-1, +J \quad (2.22)$$

Additionally, there are no matrix elements that couple between odd/even K states, so may be solved separately. The oddness or evenness of the K value can be linked to the ortho or para states of water, as they fulfill the symmetry requirement for the respective wavefunctions. The ortho states of water are related to odd K symmetric top states, and as mentioned in the introduction corresponds to a total nuclear spin of 1, (the spins of the hydrogen nuclei are parallel). Para water relates to states with even K, and corresponds to hydrogen nuclear spins being anti-parallel and thus a total nuclear spin of 0.

This block Hamiltonian may be diagonalized in order to produce an energy level diagram such as in Figure 1. The level splitting of the ground-state ortho level mentioned previously is within the M degeneracy. The M quantum number corresponds to the space-fixed projection of the molecule, which is why the lifting of this degeneracy is a signature of an anisotropic environment as the space-fixed projection is no longer equivalent in all

directions.

2.2.1 Contribution to Thermodynamic Energy

The rotational thermodynamic energy was plotted for a range of temperatures in the figure below.

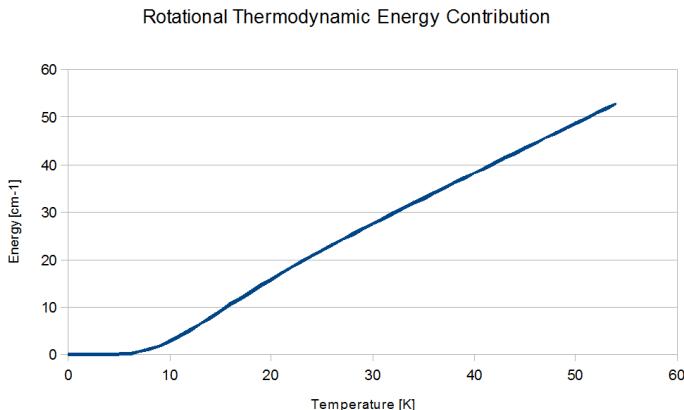


Figure 5: Rotational Contribution to Thermodynamic Energy

2.3 Exact Imaginary Time Orientation Autocorrelation Functions

One property of the endohedral water that will be interesting to look at is the imaginary time orientation autocorrelation function. This exact correlation function can be computed for a free water and subsequently compared to the caged water to investigate the caging effect. Imaginary time autocorrelation functions have several features including: they are symmetric about $\tau = \frac{\beta}{2}$. At very low temperature the ITACFs generally decay to 0 by the midpoint and have a wide β range, representing a very quantum-like system. At high temperature the ITACFs reduce to a single point at (1,0) as the β range is effectively 0, meaning the molecule remains perfectly correlated in τ - imaginary time and represents a more classical-like object. The operator associated with the orientation is a vector repre-

senting a specific axis of interest. The three main vectors that we will be interested in are the three principal axis of the molecule, V_x , V_y , and V_z , where these vectors in the space fixed frame are given by each column in the rotation matrix:

$$R = \begin{pmatrix} \cos \phi \cos \theta \cos \chi - \sin \phi \sin \chi & -\cos \phi \cos \theta \sin \chi - \sin \phi \cos \chi & \cos \phi \sin \theta \\ \sin \phi \cos \theta \cos \chi + \cos \phi \sin \chi & -\sin \phi \cos \theta \sin \chi + \cos \phi \cos \chi & \sin \phi \sin \theta \\ -\sin \theta \cos \chi & \sin \theta \sin \chi & \cos \theta \end{pmatrix} \quad (2.23)$$

In order to calculate the ITACF for these vectors, we must modify the expression obtained above slightly. Beginning with:

$$\frac{1}{Z} \sum_n \sum_\gamma e^{-\beta E_n} e^{\frac{\tau(E_n - E_\gamma)}{\hbar}} \langle n | \hat{O} | \gamma \rangle \langle \gamma | \hat{O} | n \rangle \quad (2.24)$$

we may insert four complete sets of JKM states and expand.

$$\begin{aligned} & \frac{1}{Z} \sum_n \sum_\gamma \sum_{JKM} \sum_{J'K'M'} \sum_{J''K''M''} \sum_{J'''K'''M'''} e^{-\beta E_n} e^{\frac{\tau(E_n - E_\gamma)}{\hbar}} \\ & \langle n | JKM \rangle \langle JKM | \hat{O} | J'K'M' \rangle \langle J'K'M' | \gamma \rangle \\ & \langle \gamma | J''K''M'' \rangle \langle J''K''M'' | \hat{O} | J'''K'''M''' \rangle \langle J'''K'''M''' | n \rangle \end{aligned}$$

We can take measures to simplify this equation before replacing the generic operator \hat{O} with the directions of interest. As mentioned previously, the eigenvalues of the asymmetric top in the JKM basis are good quantum numbers in J and M, and are only mixed in K. That means that $\langle n | JKM \rangle$ and $\langle J'''K'''M''' | n \rangle$ may be simplified since J will always equal J''' , and M will always equal M''' . Likewise for the second energy state sums, the J' and M' will always equal J'' and M'' , respectively. Also, we will write the projection of the

energy state on the JKM basis as C_n^{JKM} .

$$\frac{1}{Z} \sum_n \sum_\gamma e^{-\beta E_n} e^{\frac{\tau(E_n - E_\gamma)}{\hbar}} \sum_{JM} \sum_{J'M'} \sum_K \sum_{K'} \sum_{K''} \sum_{K'''} C_n^{JKM} C_\gamma^{J'K'M'} C_\gamma^{J'K''M'} C_n^{JK'''M} \langle JKM | \hat{O} | J'K'M' \rangle \langle J'K''M' | \hat{O} | JK'''M \rangle$$

The use of quadratures in the evaluation of the matrix elements $\langle JKM | \hat{O} | J'K'M' \rangle$ may be avoided if we recognize that the orientation vectors can be written in terms of Wigner-D rotation matrices. This process is omitted here and left to Appendix A, but the results will be shown.

For $\hat{O} = V_x$ we find:

$$\begin{aligned} & \langle JKM | V_x | J'K'M' \rangle \langle J'K''M' | V_x | JK'''M \rangle \\ &= \langle jk_1m | [-\frac{1}{\sqrt{2}}(D_{q1}^1 - D_{q-1}^1)] | j'k'_1m' \rangle \langle j'k'_2m' | [-\frac{1}{\sqrt{2}}(D_{q1}^{1*} - D_{q-1}^{1*})] | jk_2m \rangle \\ &= (-1)^{m+m'-k'_1-k_2} \frac{(2J+1)(2J'+1)}{2} \left[\begin{pmatrix} J & 1 & J' \\ k_1 & 1 & -k'_1 \end{pmatrix} - \begin{pmatrix} J & 1 & J' \\ k_1 & -1 & -k'_1 \end{pmatrix} \right] \\ & \times \left[\begin{pmatrix} J' & 1 & J \\ k'_2 & -1 & -k_2 \end{pmatrix} - \begin{pmatrix} J' & 1 & J \\ k'_2 & 1 & -k_2 \end{pmatrix} \right] \sum_q (-1)^{q+1} \begin{pmatrix} J & 1 & J' \\ M & q & -M' \end{pmatrix} \begin{pmatrix} J' & 1 & J \\ M' & -q & -M \end{pmatrix} \end{aligned}$$

for $\hat{O} = V_y$ we find:

$$\begin{aligned}
& \langle JKM | V_y | J'K'M' \rangle \langle J'K''M' | V_y | JK'''M \rangle \\
& = \langle jk_1m | [\frac{i}{\sqrt{2}}(D_{q1}^1 + D_{q-1}^1)] | j'k'_1m' \rangle \langle j'k'_2m' | [-\frac{i}{\sqrt{2}}(D_{q1}^{1*} + D_{q-1}^{1*})] | jk_2m \rangle \\
& = (-1)^{m+m'-k'_1-k_2} \frac{(2J+1)(2J'+1)}{2} \left[\begin{pmatrix} J & 1 & J' \\ k_1 & 1 & -k'_1 \end{pmatrix} + \begin{pmatrix} J & 1 & J' \\ k_1 & -1 & -k'_1 \end{pmatrix} \right] \\
& \times \left[\begin{pmatrix} J' & 1 & J \\ k'_2 & -1 & -k_2 \end{pmatrix} + \begin{pmatrix} J' & 1 & J \\ k'_2 & 1 & -k_2 \end{pmatrix} \right] \sum_q (-1)^{q+1} \begin{pmatrix} J & 1 & J' \\ M & q & -M' \end{pmatrix} \begin{pmatrix} J' & 1 & J \\ M' & -q & -M \end{pmatrix}
\end{aligned}$$

and for $\hat{O} = V_z$ we find:

$$\begin{aligned}
& \langle JKM | V_z | J'K'M' \rangle \langle J'K''M' | V_z | JK'''M \rangle \\
& = \langle jk_1m | D_{q0}^1 | j'k'_1m' \rangle \langle j'k'_2m' | D_{q0}^{1*} | jk_2m \rangle \\
& = (-1)^{m+m'-k'_1-k_2} (2J+1)(2J'+1) \begin{pmatrix} J & 1 & J' \\ k_1 & 0 & -k'_1 \end{pmatrix} \begin{pmatrix} J' & 1 & J \\ k'_2 & 0 & -k_2 \end{pmatrix} \\
& \times \sum_q (-1)^q \begin{pmatrix} J & 1 & J' \\ M & q & -M' \end{pmatrix} \begin{pmatrix} J & 1 & J' \\ M' & -q & -M \end{pmatrix}
\end{aligned}$$

Using these formulas, the exact orientational imaginary time autocorrelation function was plotted for water at 4K, 12K and 55K in the following figures. It is interesting here to note that each V_a , V_b and V_c was found to uniquely couple from the ground rotational $J=0$ state, to an excited $J=1$ state. The V_a was found to be the only operator to couple the ground *para* state to the ground *ortho* state, 1_{10} . In addition, each spherical component

of the V_a vector couples to a different M level in the triply degenerate ground state. Thus, it should in theory be possible to determine the splitting as measured in experiment by looking at the imaginary time autocorrelation functions obtained through simulations, as any change in the energy level directly affects the ITACF.

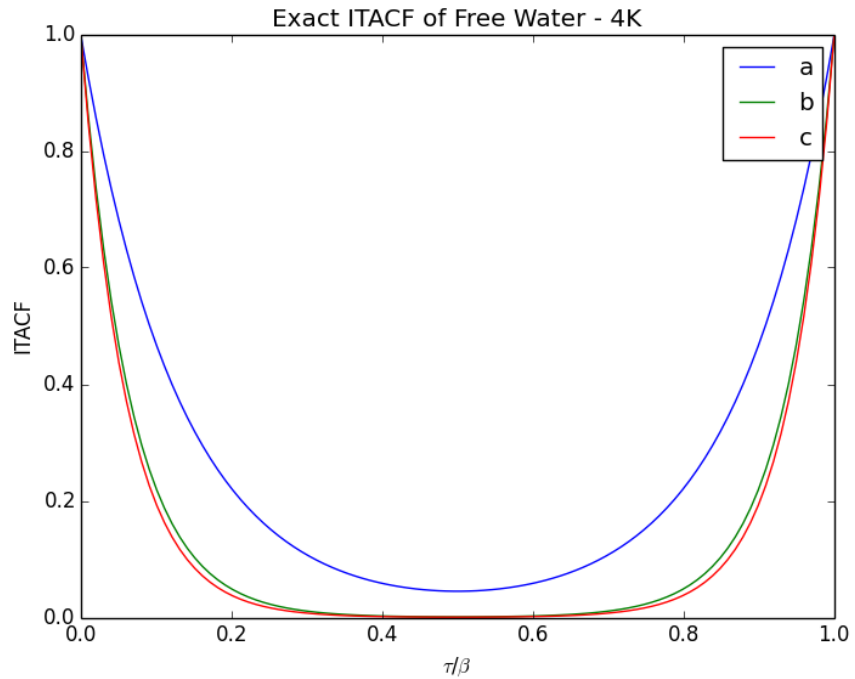


Figure 6: Exact ITACF of H₂O, T=4K

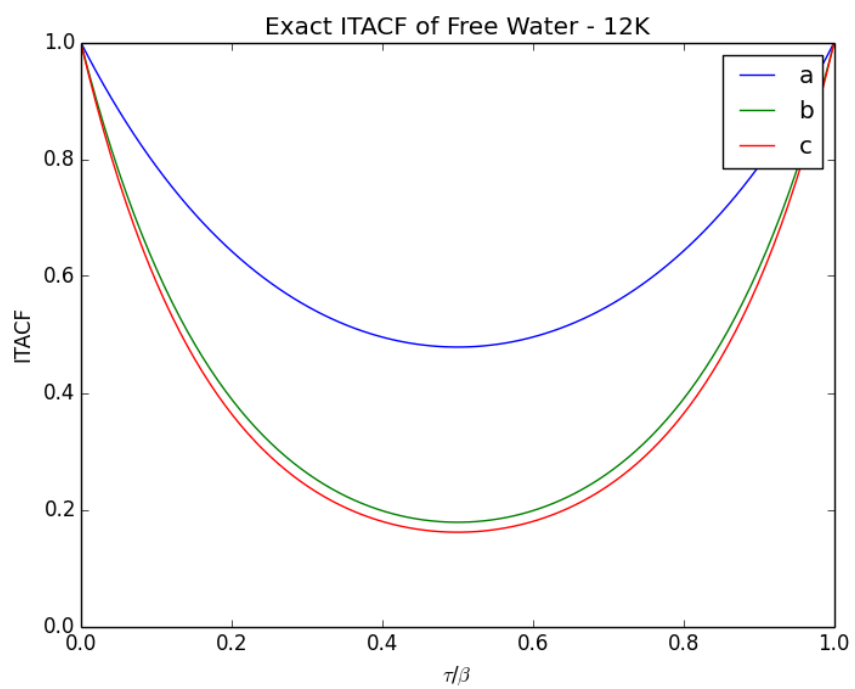


Figure 7: Exact ITACF of H₂O, T=12K

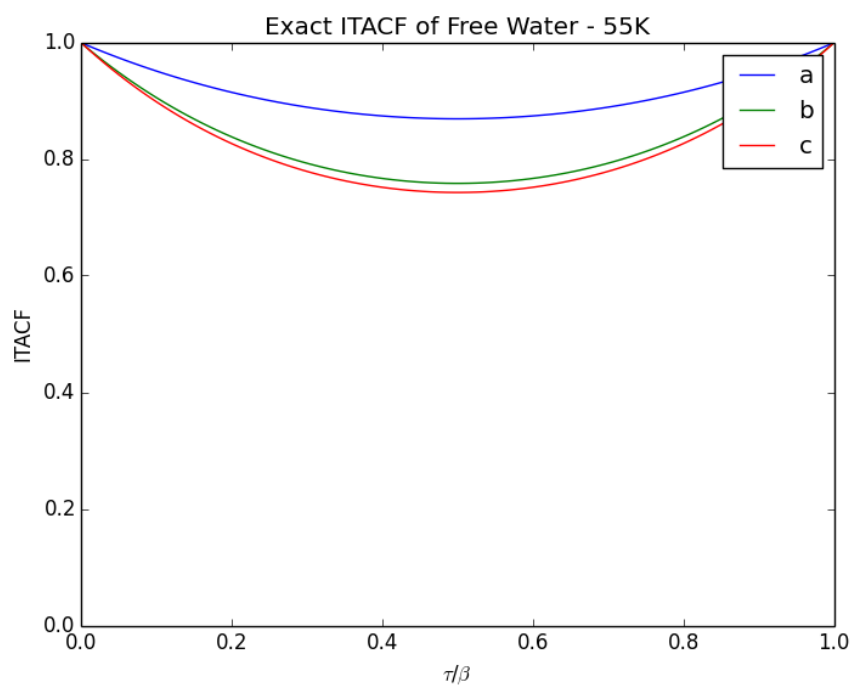


Figure 8: Exact ITACF of H₂O, T=55K

Chapter 3

Path Integral Molecular Dynamics

Path Integral Molecular Dynamics (PIMD) is a technique that was developed based on Feynman path integrals and provides us with a powerful tool to sample quantum mechanical distributions.²³

3.1 Path Integral Formulation of the Partition Function

In order to formulate the equations of motion for PIMD, we may first begin by writing the canonical partition function in the coordinate basis.

$$Z = \int d\mathbf{q} \langle \mathbf{q} | e^{-\beta \hat{H}} | \mathbf{q} \rangle \quad (3.1)$$

$$Z = \int d\mathbf{q} \langle \mathbf{q} | e^{-\beta(\hat{K}+\hat{U})} | \mathbf{q} \rangle .$$

Where \hat{H} represents the Hamiltonian, and \hat{K} and \hat{U} are the kinetic and potential energy operators respectively. Unfortunately, the operators \hat{K} and \hat{U} do not commute, and we require the use of the Trotter Theorem, allowing us to replace the operator

$$e^{-\beta(\hat{K}+\hat{U})} = \lim_{P \rightarrow \infty} [e^{-\beta\hat{U}/2P} e^{-\beta\hat{K}/P} e^{-\beta\hat{U}/2P}]^P$$

We see that the partition function, upon introduction of the operator

$$\hat{\Omega} = e^{-\beta\hat{U}/2P} e^{-\beta\hat{K}/P} e^{-\beta\hat{U}/2P}$$

can be written

$$Z = \lim_{P \rightarrow \infty} \int d\mathbf{q} \langle \mathbf{q} | \hat{\Omega}^P | \mathbf{q} \rangle = \int d\mathbf{q} \langle \mathbf{q} | \hat{\Omega} \hat{\Omega} \dots \hat{\Omega} | \mathbf{q} \rangle.$$

The next step is to insert $P - 1$ resolution of the identity operator's

$$\hat{I} = \int d\mathbf{q} |\mathbf{q}\rangle \langle \mathbf{q}|$$

in between the P number of $\hat{\Omega}$'s, giving us

$$\begin{aligned} Z &= \lim_{P \rightarrow \infty} \int d\mathbf{q}_1 \dots d\mathbf{q}_P \times \langle \mathbf{q}_1 | \hat{\Omega} | \mathbf{q}_2 \rangle \langle \mathbf{q}_2 | \dots | \mathbf{q}_P \rangle \langle \mathbf{q}_P | \hat{\Omega} | \mathbf{q}_{P+1} \rangle \\ &= \lim_{P \rightarrow \infty} \int d\mathbf{q}_1 \dots d\mathbf{q}_P \prod_{i=1}^P \left[\langle \mathbf{q}_i | \hat{\Omega} | \mathbf{q}_{i+1} \rangle \right]_{q_{P+1}=q_1} \end{aligned}$$

Since \hat{U} is a function of $\hat{\mathbf{q}}$, $|\mathbf{q}\rangle$'s are eigenvectors of \hat{U} with eigenvalues $e^{-\beta U_{\mathbf{q}}/2P}$. The result is that our matrix element

$$\langle \mathbf{q}_i | \hat{\Omega} | \mathbf{q}_{i+1} \rangle = \langle \mathbf{q}_i | e^{-\beta\hat{U}/2P} e^{-\beta\hat{K}/P} e^{-\beta\hat{U}/2P} | \mathbf{q}_{i+1} \rangle$$

can be reduced to

$$\langle \mathbf{q}_i | \hat{\Omega} | \mathbf{q}_{i+1} \rangle = e^{-\beta U(\mathbf{q}_i)/2P} \langle \mathbf{q}_i | e^{-\beta\hat{K}/P} | \mathbf{q}_{i+1} \rangle e^{-\beta U(\mathbf{q}_{i+1})/2P}.$$

Now, we insert P resolutions of the identity operator, this time in terms of momentum eigenvectors,

$$\hat{I} = \int d\mathbf{p} |\mathbf{p}\rangle\langle\mathbf{p}|$$

within each matrix element.

$$\langle\mathbf{q}_i| e^{-\beta\hat{K}/P} |\mathbf{q}_{i+1}\rangle = \int d\mathbf{p} \langle\mathbf{q}_i| e^{-\beta\hat{K}/P} |\mathbf{p}\rangle \langle\mathbf{p}|\mathbf{q}_{i+1}\rangle$$

We can see now that the operator, a function of the momentum operator, is acting on its eigenvector $|\mathbf{p}\rangle$, so this is reduced to

$$\langle\mathbf{q}_i| e^{-\beta\hat{K}/P} |\mathbf{q}_{i+1}\rangle = \int d\mathbf{p} \langle\mathbf{q}_i|\mathbf{p}\rangle \langle\mathbf{p}|\mathbf{q}_{i+1}\rangle e^{-\beta\mathbf{p}^2/2mP}$$

$$\langle\mathbf{q}_i| e^{-\beta\hat{K}/P} |\mathbf{q}_{i+1}\rangle = \left(\frac{1}{2\pi\hbar}\right)^3 \int d\mathbf{p} e^{-\beta\mathbf{p}^2/2mP} e^{i\mathbf{p}(\mathbf{q}_i - \mathbf{q}_{i+1})/\hbar}$$

After completing the square and integrating over $\mathbf{p} \in (-\infty, \infty)$, we determine that

$$\langle\mathbf{q}_i| e^{-\beta\hat{K}/P} |\mathbf{q}_{i+1}\rangle = \left(\frac{mP}{2\pi\beta\hbar^2}\right)^{3/2} \exp\left[-\frac{mP}{2\beta\hbar^2}(\mathbf{q}_i - \mathbf{q}_{i+1})^2\right]$$

we see that the partition function matrix element is simply

$$\langle\mathbf{q}_i|\hat{\Omega}|\mathbf{q}_{i+1}\rangle = \left(\frac{mP}{2\pi\beta\hbar^2}\right)^{3/2} \exp\left[-\frac{mP}{2\beta\hbar^2}(\mathbf{q}_i - \mathbf{q}_{i+1})^2\right] \times \exp\left[-\frac{\beta}{2P}(U(\mathbf{q}_i) + U(\mathbf{q}_{i+1}))\right]$$

After resubstituting this expression, we are required to set $\mathbf{q}_1 = \mathbf{q}_{P+1}$ since it is a trace.

This means that the path is closed, thereby obtaining

$$Z = \lim_{P \rightarrow \infty} \left(\frac{mP}{2\pi\beta\hbar^2} \right)^{3P/2} \int d\mathbf{q}_1 \dots d\mathbf{q}_P \times \exp \left[-\frac{1}{\hbar} \sum_{i=1}^P \left(\frac{mP}{2\beta\hbar} (\mathbf{q}_i - \mathbf{q}_{i+1})^2 + \frac{\beta\hbar}{P} U(\mathbf{q}_i) \right) \right]_{\mathbf{q}_{P+1}=\mathbf{q}_1}$$

This is the path integral formulation of the partition function. If we remove the limit as $P \rightarrow \infty$, we obtain the discretized partition function Z_P .

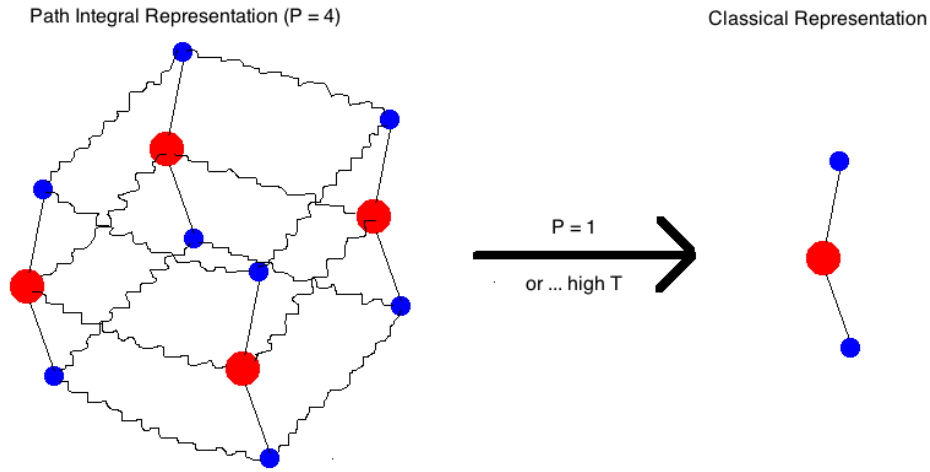


Figure 9: Path Integral Representation of Water: this figure shows us how we may interpret the path integral representation of a water molecule. The solid lines represent atomic potential interactions within a single molecule, and the squiggly lines represent the spring potential between beads.

From Figure 9, it can be seen that the path integral representation reproduces our classical result in the case $P = 1$ (P is the number of slices that we discretized our closed path with). Additionally, it can be shown that in the high T limit, as $T \rightarrow \infty, \beta \rightarrow 0$, in which case the spring constant also approaches ∞ , once again recovering the classical view of one “bead”.

3.2 Thermodynamic Estimators

In order to extract thermodynamic properties from the PIMD simulation, functions that are referred to as “estimators” must be used. “Estimators” are functions whose average is equivalent to the value of the actual physical observable. It is fairly easy to derive these estimators from statistical mechanics, although they may exhibit horrendous convergence properties due to very large fluctuations in the data. As such, simulations must usually be run for a long time in order to ensure small errors. The estimators of utmost importance are the energy estimators. There are two that were used in this work including the primitive energy estimator, and the virial energy estimator, both of which are described below.

From statistical mechanics, we know that the energy of the system is equivalent to the negative derivative of the logarithm of the partition function with respect to β .

$$E = -\frac{d}{d\beta} (\ln Z) \quad (3.2)$$

We are able to evaluate this directly by substituting in the discretized path integral formulation for the partition function that we arrived at previously. After substituting in Z_P , it can be seen that the energy estimator may be written as

$$E_{prim} = \frac{3P}{2\beta} - \sum_{i=1}^P \frac{mP}{2\beta^2\hbar^2} (\mathbf{q}_{i+1} - \mathbf{q}_i)^2 + \frac{1}{P} \sum_{i=1}^P U(\mathbf{q}_i) \quad (3.3)$$

This particular version of the energy estimator is referred to as the Primitive Energy Estimator, in comparison to the Virial Estimator that can be found by applying the virial theorem.²⁴ The virial energy estimator has the form:

$$E_{vir} = \frac{3P}{2\beta} + \sum_{i=1}^P \frac{1}{2} (\mathbf{q}_i - \mathbf{q}_{centroid}) \cdot \frac{\delta U}{\delta \mathbf{q}_i} + \frac{1}{P} \sum_{i=1}^P U(\mathbf{q}_i) \quad (3.4)$$

Molecular Modelling Toolkit

All of the PIMD simulations that are conducted are done within the framework of The Molecular Modelling Toolkit (MMTK).²⁵ MMTK is an opensource library that was written by Konrad Hinzen, in Python, C, and Cython. The basis behind MMTK was to provide a new platform to conduct molecular simulations, through the easy-to-learn programming language Python. The main step in order to implement MMTK is constructing a force field that is responsible for modelling the interaction between constituents of the system. The force field interactions are taken into consideration when calculating the forces that determine the equations of motion.

Path Integral Langevin Equation

The Path Integral Langevin Equation (PILE)²⁶ is a method used to thermostat a system, and so allows sampling from the canonical ensemble (NVT). It was shown previously that the Langevin equation could be combined with the Velocity Verlet algorithm,²⁷ and since PIMD is based off of classical equations of motion that can be computed with the Velocity Verlet method, it was soon after adapted to be used in conjunction with PIMD.

3.3 Parameter Optimization

In order to efficiently use PIMD and have statistically relevant data, there are three parameters that need to be optimized beforehand: the centroid friction coefficient, simulation timestep, and the number of beads (ie. τ parameter).

3.3.1 Centroid Friction Coefficient

The centroid friction coefficient is related to how the PILE thermostats the PIMD simulation. This parameter must be optimized in order to increase sampling efficiency. In

practice, the best centroid friction coefficient is the one that minimizes the decorrelation time of the observable in which we are interested. Uncorrelated data in simulation time ensures that the data are statistically independent.

In order to obtain the optimum centroid friction coefficient, the autocorrelation function was obtained for a number of observables. The autocorrelation function is completed using a Fast Fourier Transform (FFT), followed by the multiplication of the data set with its own complex conjugate, followed by an Inverse Fast Fourier Transform (IFFT), completed by the normalization of the data. There was a difficulty choosing an optimization parameter, as different properties have different decorrelation times and are optimized by different friction coefficients used in the PILE. Thus, compromises needed to be made. Figures 10, 11 and 12 highlight this, and depict the autocorrelation function for the position of the oxygen atom, as well as the orientation of the dipole. These two autocorrelation functions are compared with varying friction coefficients of 0.0 ps^{-1} , 1.0 ps^{-1} , and 100.0 ps^{-1} . In the end, 100.0 ps^{-1} was chosen as it appeared to have the best decorrelation times among all of the properties.

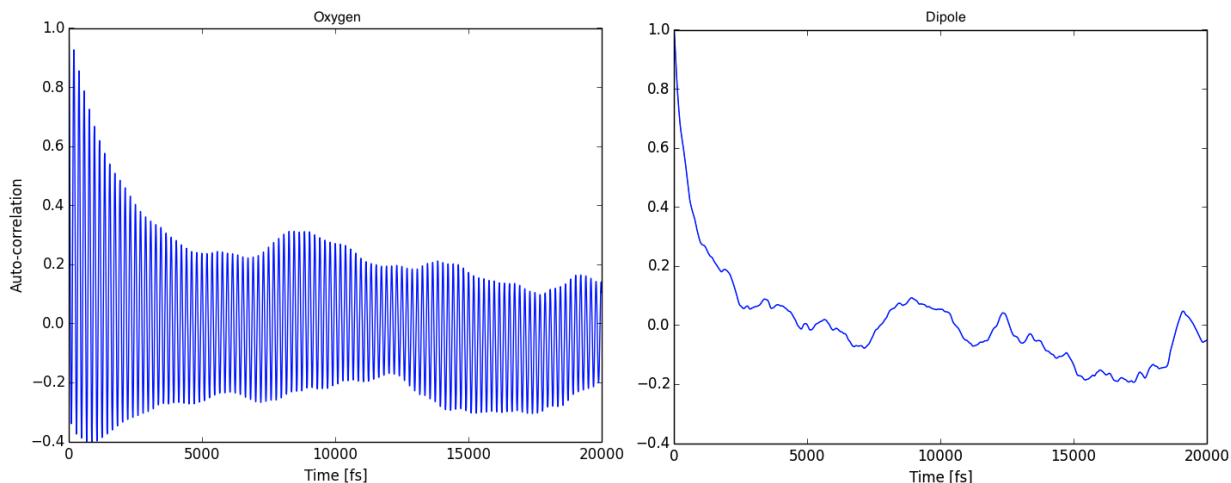


Figure 10: Auto-correlation Functions for Oxygen and Water Dipole - 0 ps^{-1}

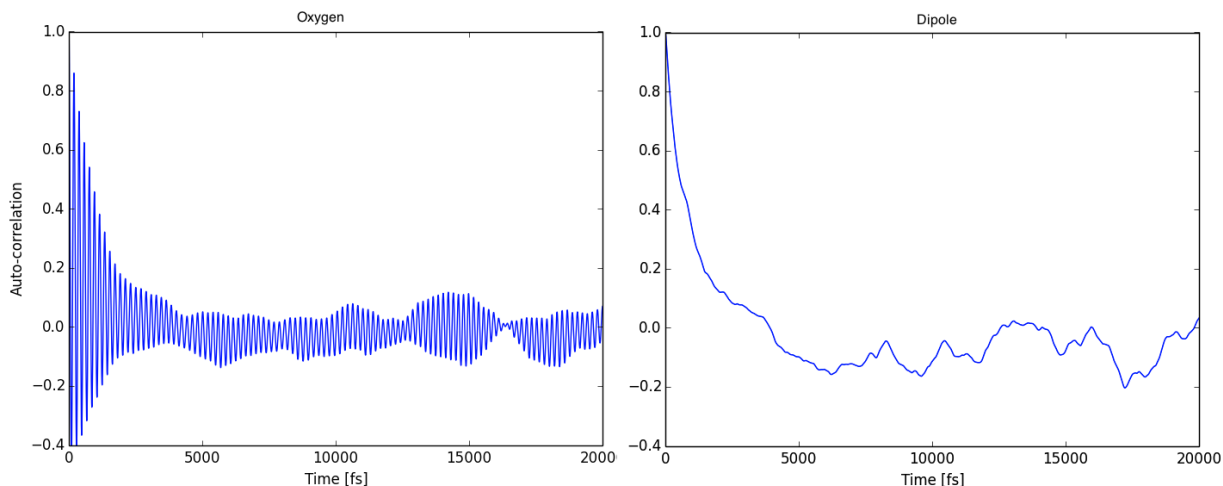


Figure 11: Auto-correlation Functions for Oxygen and Water Dipole - 1 ps^{-1}

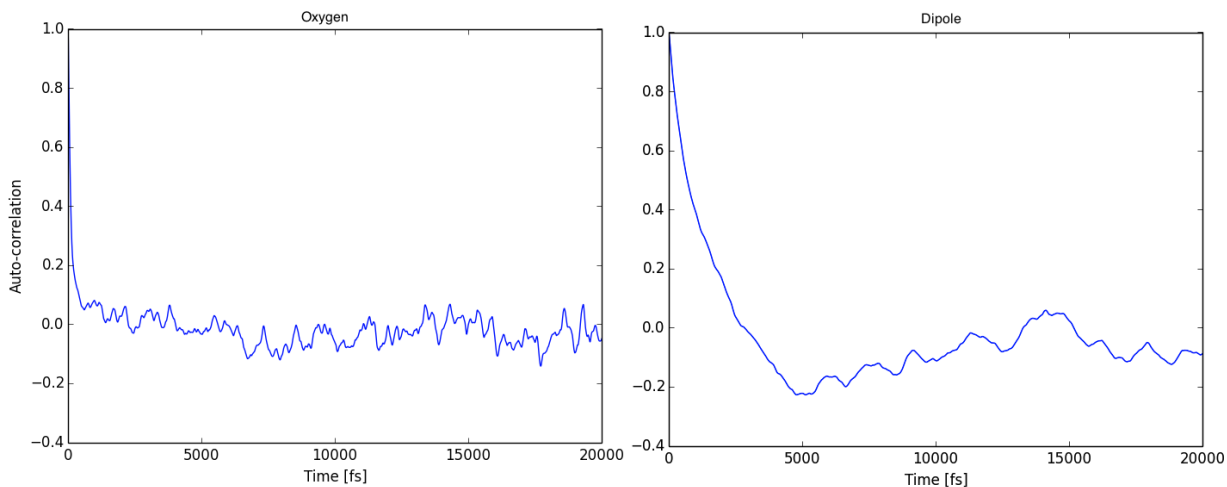


Figure 12: Auto-correlation Functions for Oxygen and Water Dipole - 100 ps^{-1}

3.3.2 Timestep

Usually long simulations are run in order to collect sufficient, uncorrelated data. In order to run a simulation for a longer “real-time”, the largest timestep possible while results remain converged is desirable. The optimal timestep was chosen by looking at the difference between the primitive and virial energy estimator, as it was noticed that these two averages diverged at too high a timestep. This can be seen in figure 13. A timestep of 0.05fs was required to ensure that the energy estimators were converged.

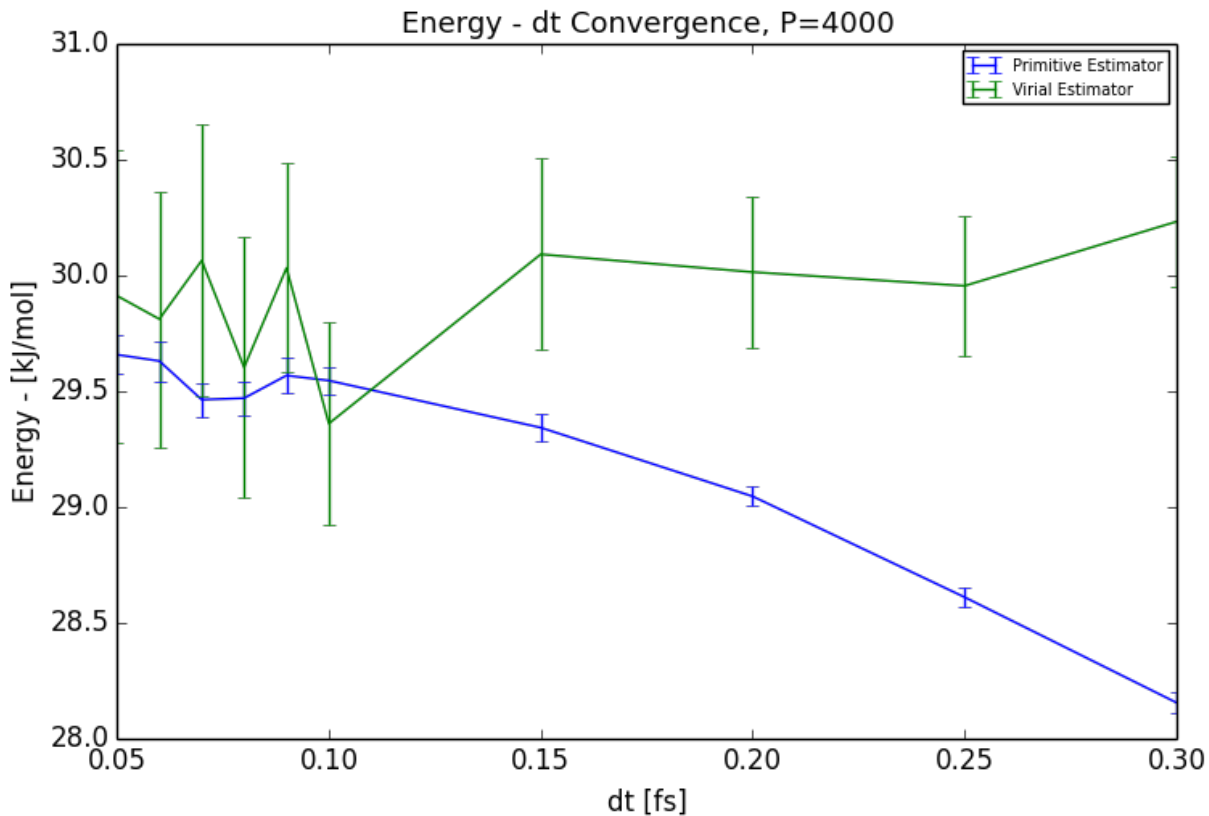


Figure 13: Timestep Convergence - Primitive vs Virial Energy Estimators

3.3.3 Energy vs. τ Convergence

The last parameter that requires optimization in PIMD simulations is the tau parameter, which can be thought of as the imaginary-time timestep. This parameter is dependent on the temperature of the system and related to the number of beads used in the simulation. Here we look at the energy convergence with respect to τ , where $\tau = \frac{\beta}{P}$. We recall that $\beta = \frac{1}{k_B T}$, and P is the number of beads. It is expected that the energy should exhibit quadratic convergence with respect to τ , which is a result of the Trotter factorization made in the development of the PIMD method. Figure 14 and 15 reflect this behaviour quite nicely.

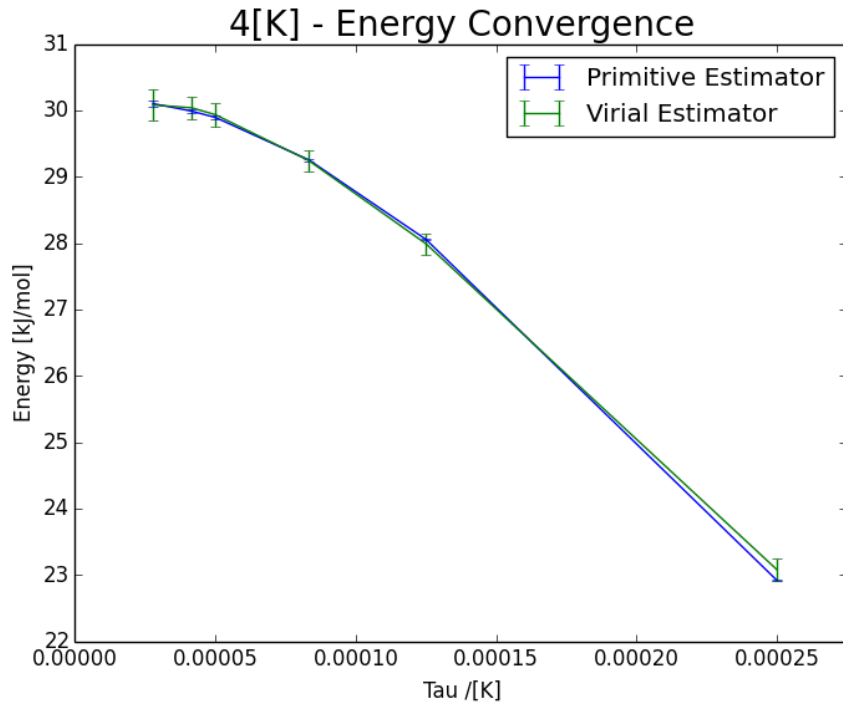


Figure 14: Energy Convergence - Primitive and Virial Energy Estimators

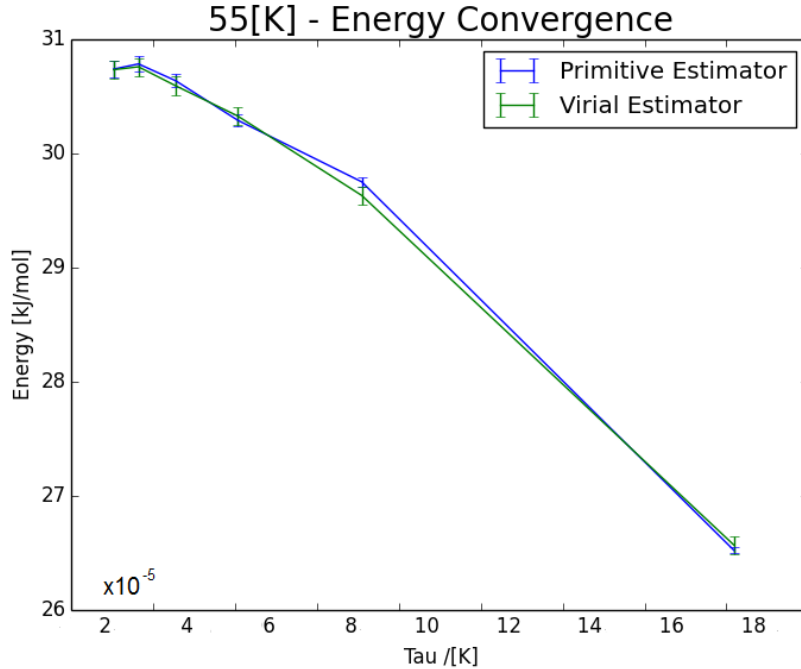


Figure 15: Energy Convergence - Primitive and Virial Energy Estimators

3.4 Density Distributions

The density distributions of several observables of the water molecule were investigated. The distributions were obtained by averaging data obtained for each bead in every output step in the simulations.

3.4.1 Center-of-Mass Position Distribution

The center-of-mass Cartesian position distributions were obtained in the x-, y-, and z-directions. This was accomplished by storing the center-of-mass of each bead of water at each decorrelated step in the simulation, over many simulations run under identical conditions. Once the data was obtained for each step in each trajectory, the data was histogrammed. The simulations were completed at a wide range of temperatures, and the trends were examined.

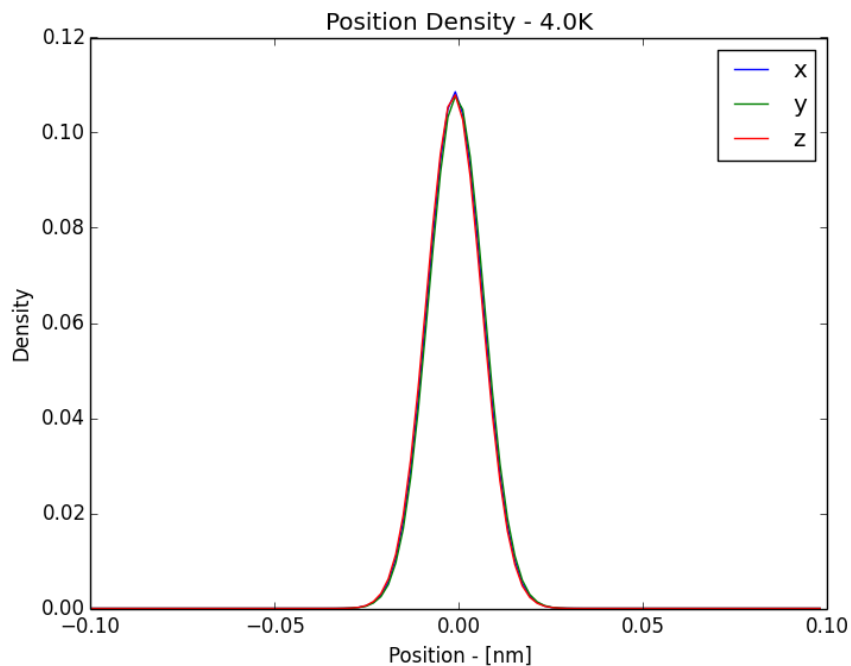


Figure 16: Center-of-Mass Density at 4K

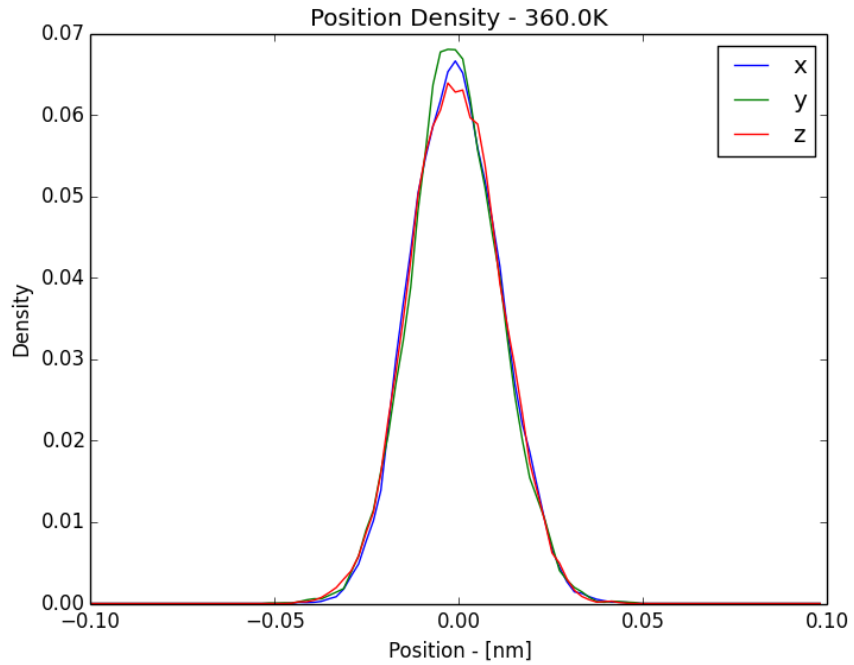


Figure 17: Center-of-Mass Density at 360K

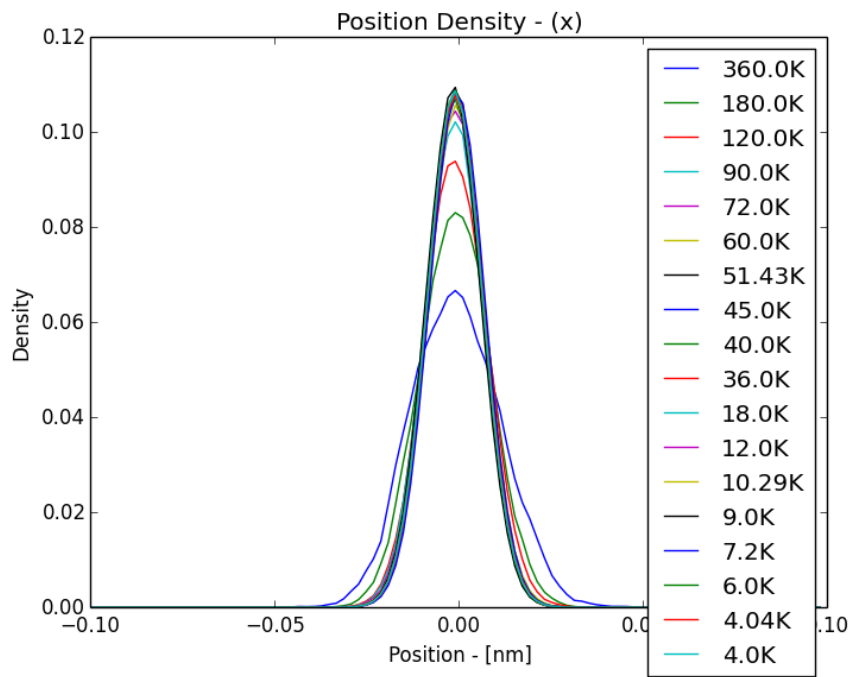


Figure 18: Center-of-Mass x-Density

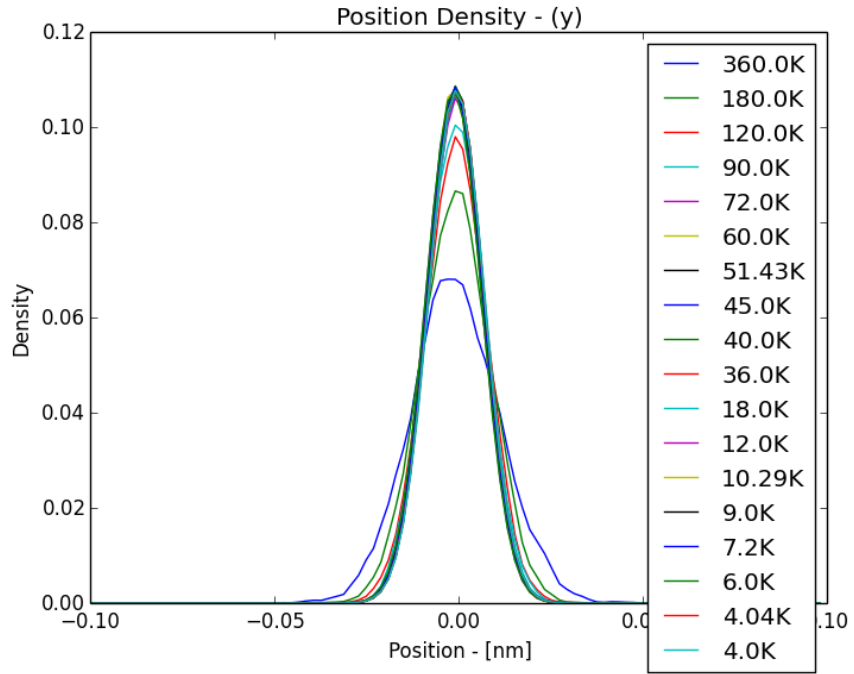


Figure 19: Center-of-Mass y-Density

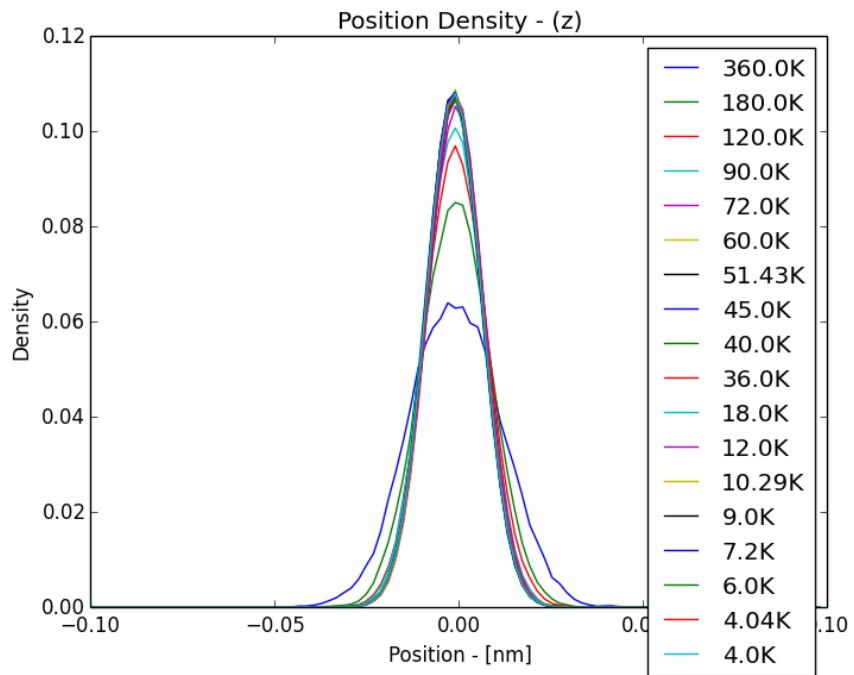


Figure 20: Center-of-Mass z-Density

Figures 16 and 17 show us that the position distribution is basically equal in the x-, y-, and z-direction, regardless of temperature, there is no temperature-dependent spatial

anisotropy. Figures 18, 19, and 20 show the temperature behaviour of these distributions in the x-, y-, and z-directions for a range of temperatures. These distributions are sharply peaked and centered about 0. They tell us that the water molecules are strongly confined within the buckyball cage, as their amplitude does not extend beyond even 0.5 Å. The center-of-mass position densities of water inside a buckyball are almost temperature independent, although at higher temperature the peaks do begin to widen.

3.4.2 Orientation Distributions

In addition to the position distributions, the orientation distributions of the water molecule in the PIMD simulations were also obtained. The specific distributions that were calculated were the ϕ and $\cos(\theta)$ distributions of each molecular principal axis of the water, with respect to spherical polar coordinates. ϕ is the azimuthal angle, and θ is the polar angle. In order to obtain the principal axes, the moment of inertia tensor was calculated and diagonalized for every bead at every timestep of interest, for each trajectory that was run. The eigenvalues of this diagonalization correspond to the principal moments of inertia, as mentioned previously. The eigenvectors correspond to the principal axis associated with the principal moment of inertia. The diagonalization method results in a random phase of the eigenvectors though, so the result may be either the positive or negative axis.

In order to correct for this polarity, three additional vectors were defined. These vectors include the dipole vector (the normalized vector along $\vec{O} - \frac{\vec{H}_1 + \vec{H}_2}{2}$). Another vector defined by $\vec{H}_2 - \vec{H}_1$ was obtained, and another by the cross product of these two. Once these three vectors were obtained the inner product with unit vectors lying along the inertial principal axes were taken. Since the inertial axis we want defined will always have a positive inner product with the vectors just defined, the phase was corrected by multiplying the diagonalized vectors by -1 to ensure this positive inner product.

Molecular Axis ϕ Distributions

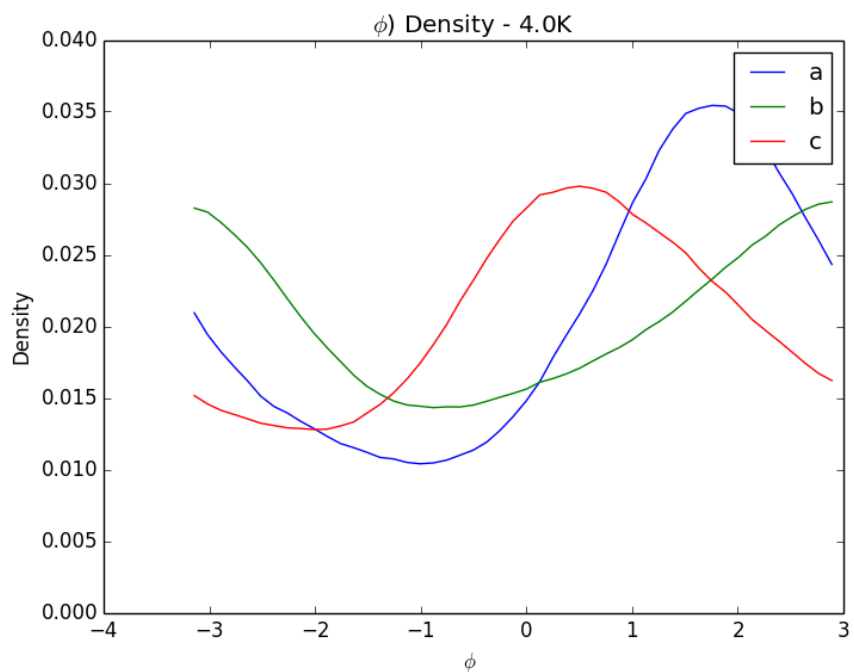


Figure 21: Principal Axis ϕ Distributions at 4K

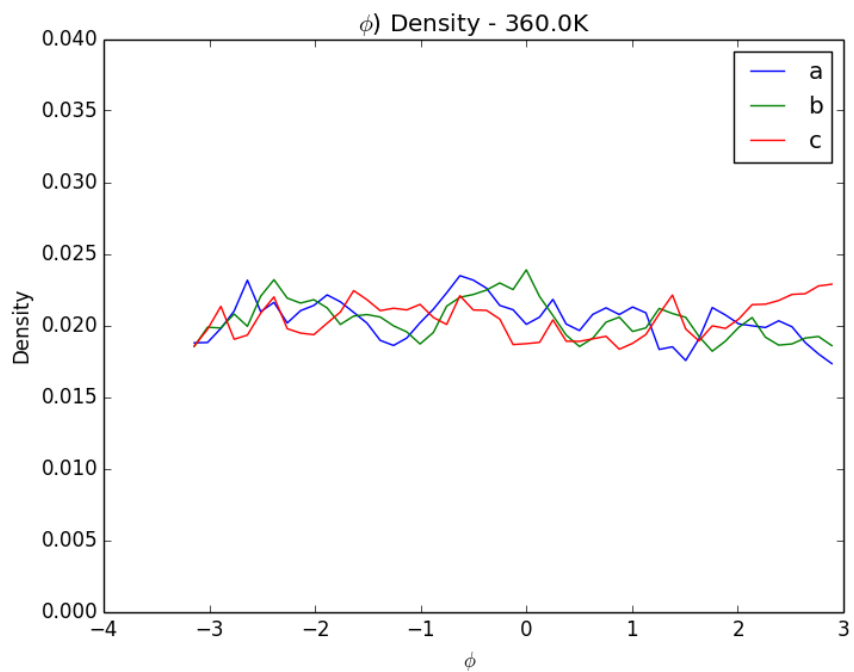


Figure 22: Principal Axis ϕ Distributions at 360K

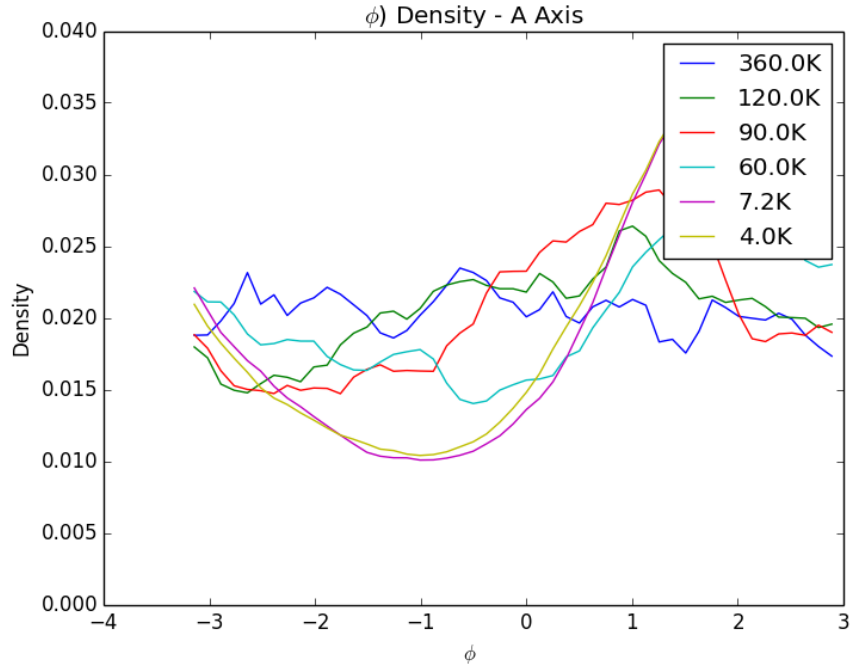


Figure 23: A-Axis ϕ Distributions

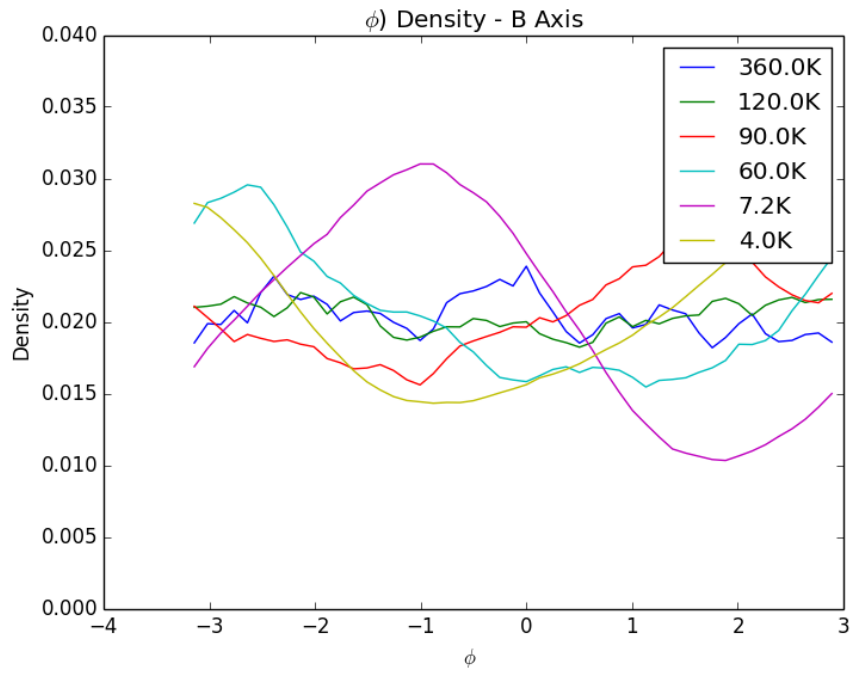


Figure 24: B-Axis ϕ Distributions

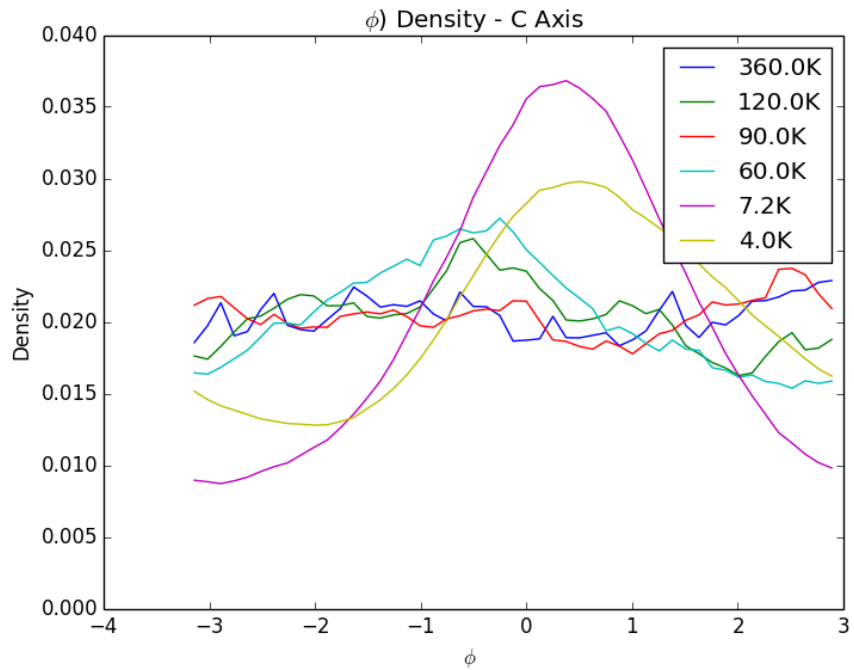


Figure 25: C-Axis ϕ Distributions

Molecular Axis $\cos(\theta)$ Distributions

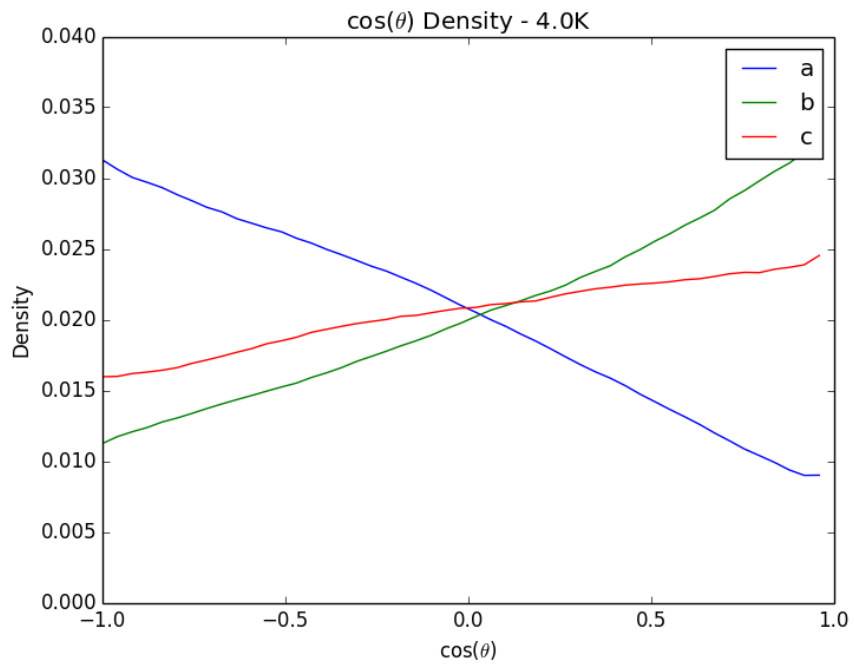


Figure 26: Principal Axis $\cos(\theta)$ Distributions at 4K

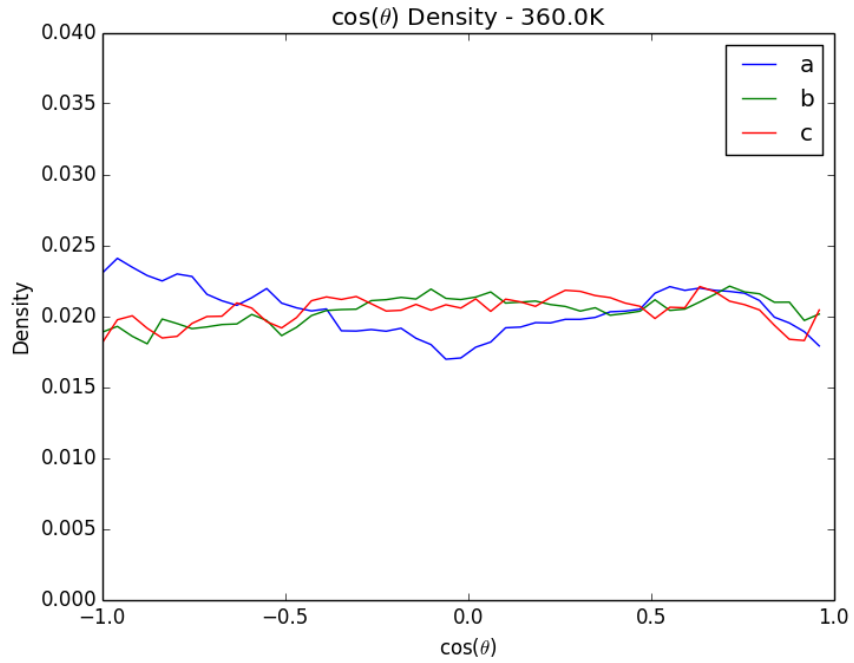


Figure 27: Principal Axis $\cos(\theta)$ Distributions at 360K

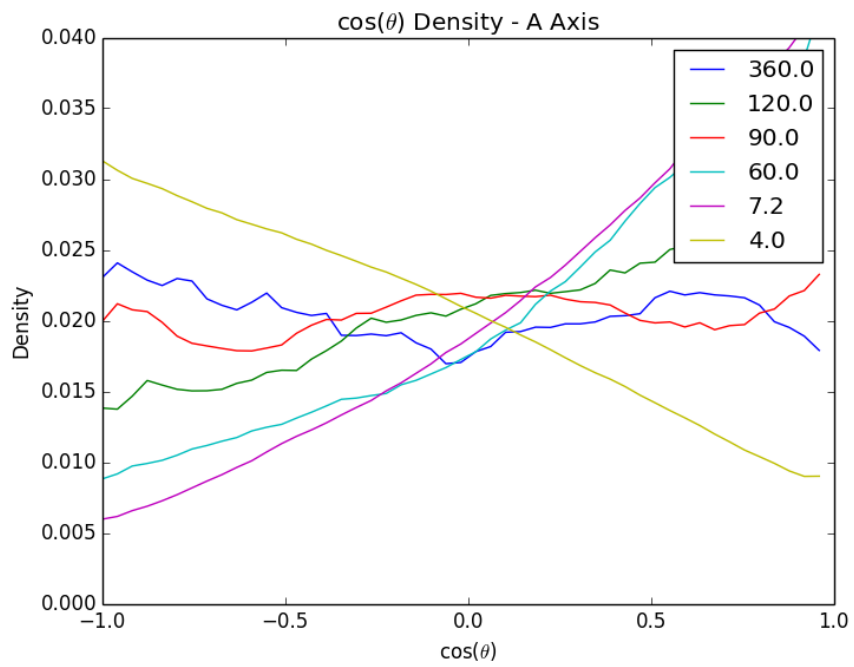


Figure 28: A-Axis $\cos(\theta)$ Distributions

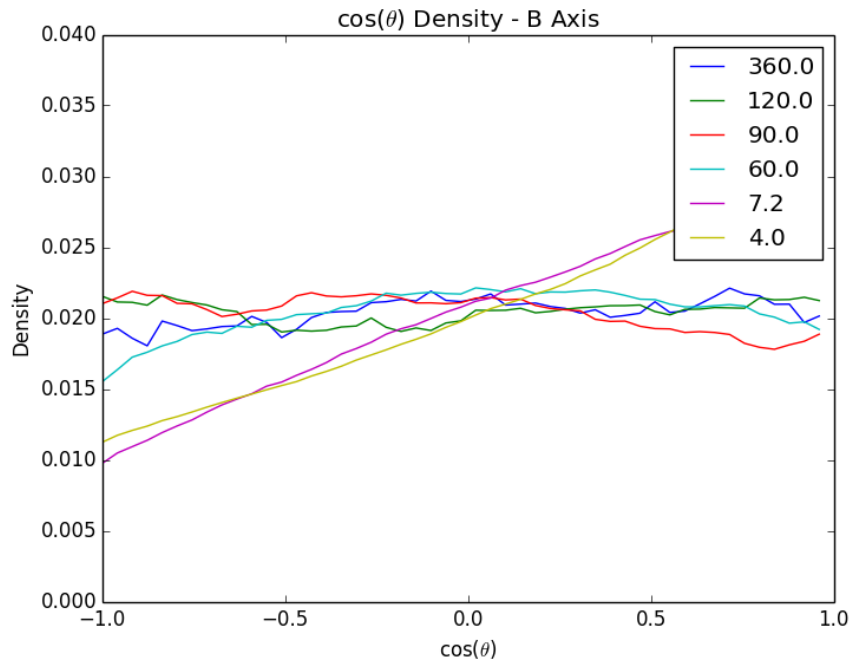


Figure 29: B-Axis $\cos(\theta)$ Distributions

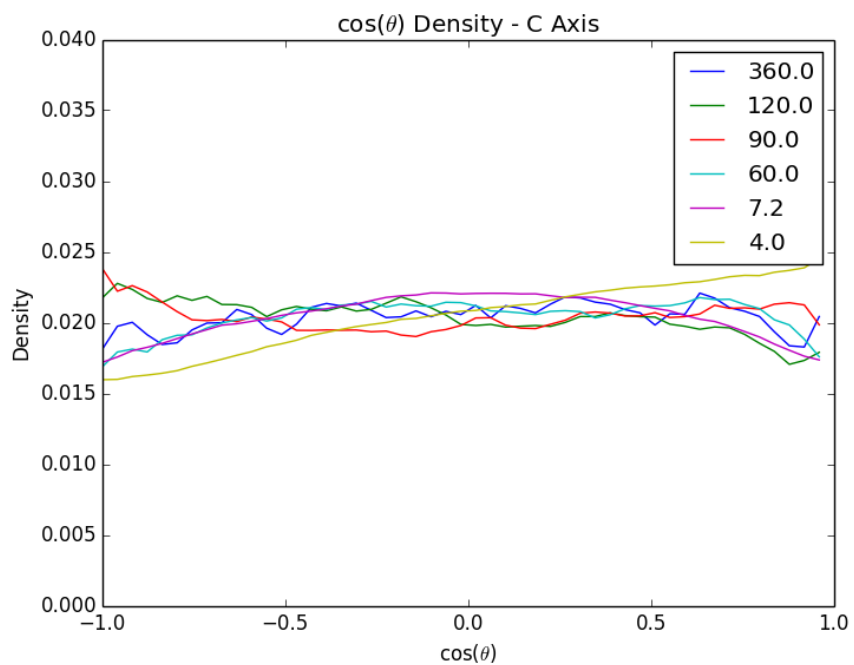


Figure 30: C-Axis $\cos(\theta)$ Distributions

These plots show that at very low temperatures, the water is much more hindered and the PIMD simulation has trouble sampling the phase-space evenly. This is an ergodicity

problem, which evidently goes away at higher temperatures. This is to be expected, as we have seen previously that the decorrelation time of the orientation of the molecule is orders of magnitude larger than that of the position. This indicates that the time-scale of rotations is much longer than that of the translational motion of the water. This leads to inefficient sampling for the properties related to orientation.

3.5 Imaginary Time Autocorrelation Functions

The behaviour of the orientational imaginary time autocorrelation functions was investigated at different temperatures, and for each molecular principal axis.

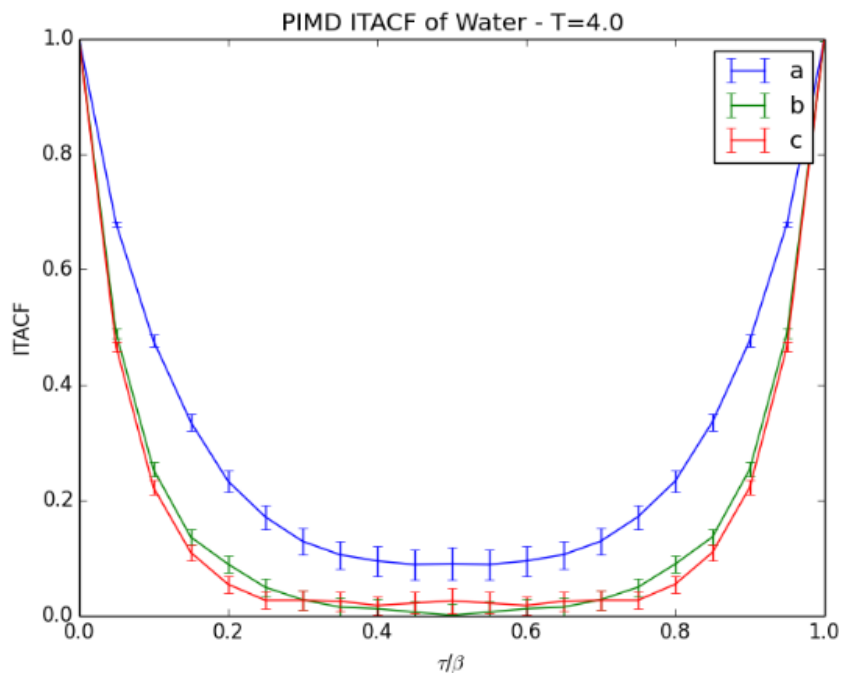


Figure 31: PIMD Orientational ITACF at 4K

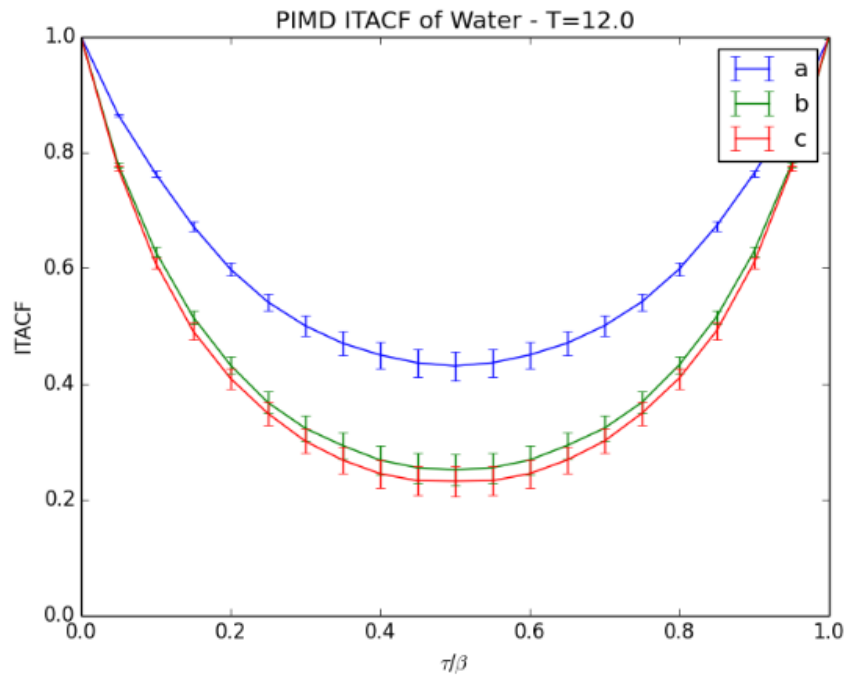


Figure 32: PIMD Orientational ITACF at 12K

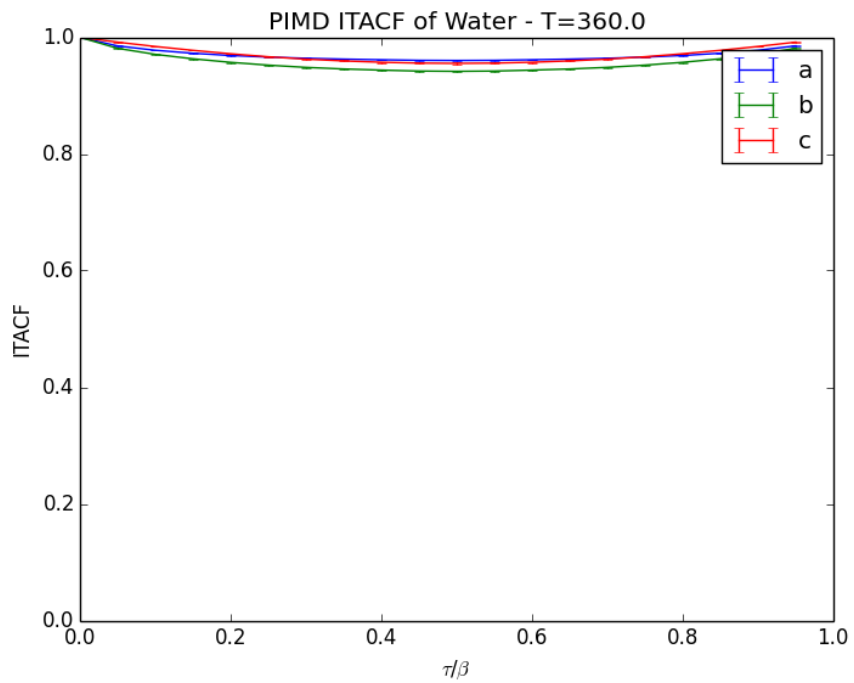


Figure 33: PIMD Orientational ITACF at 360K

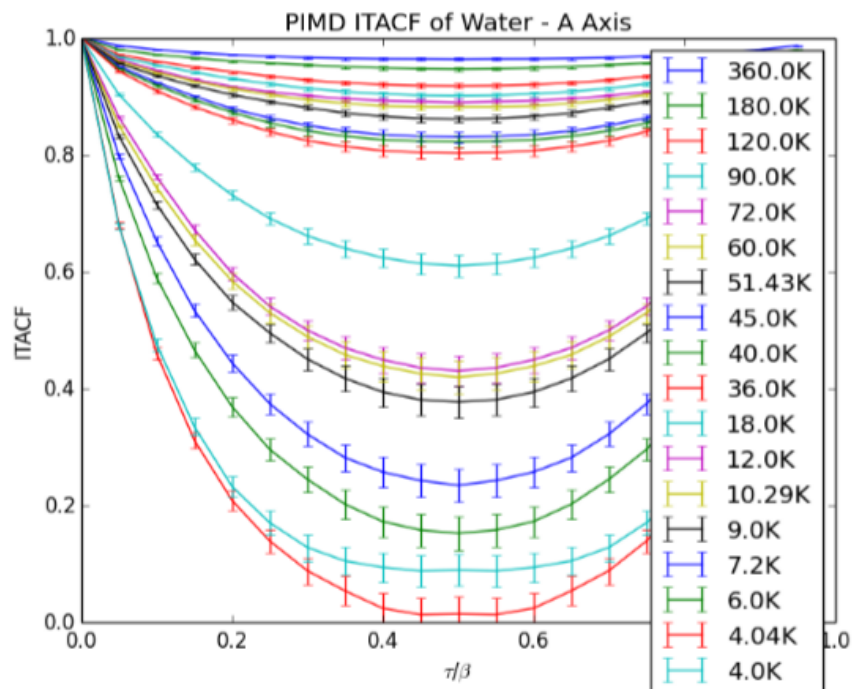


Figure 34: PIMD Orientational ITACF of A Axis

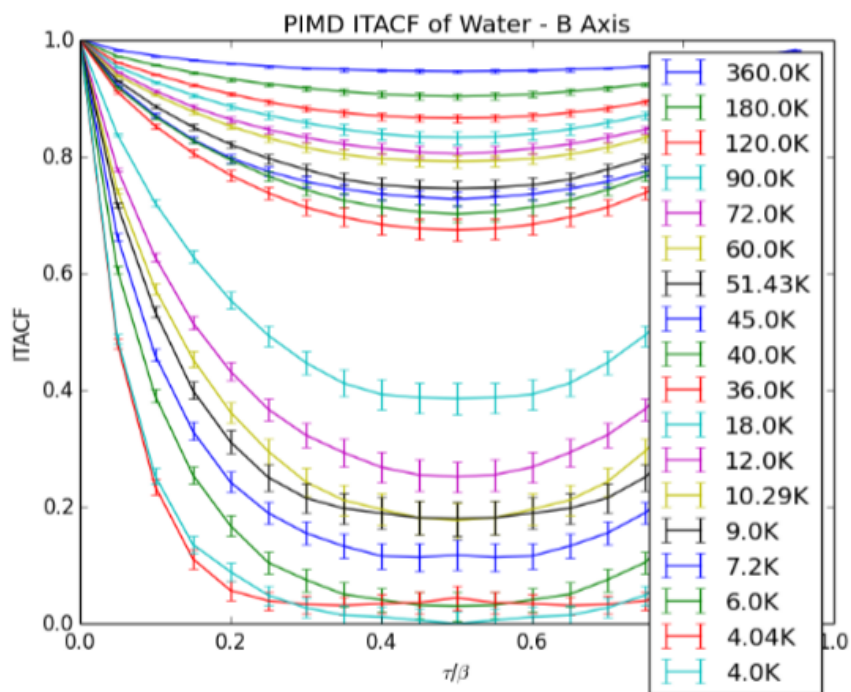


Figure 35: PIMD Orientational ITACF of B Axis

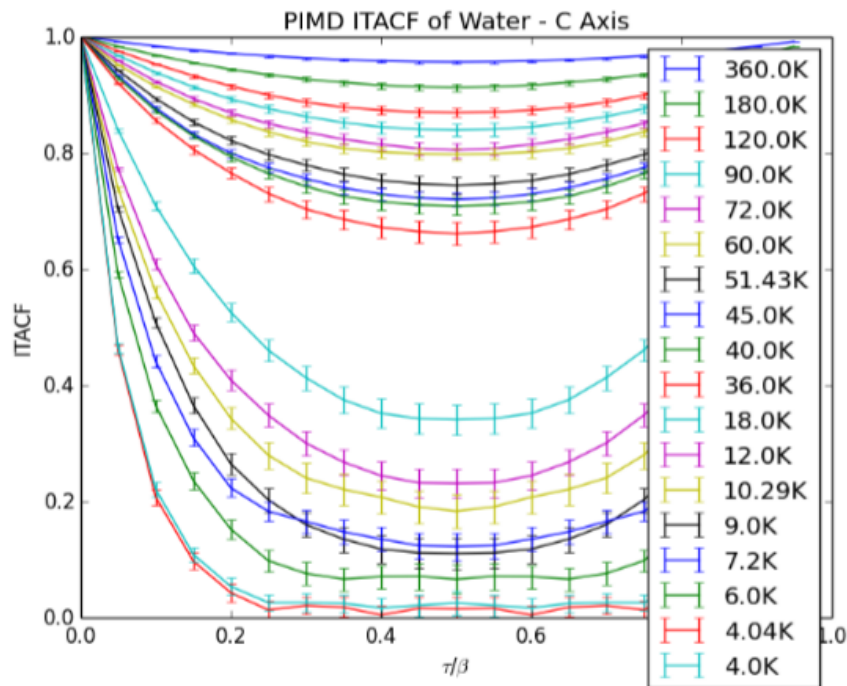


Figure 36: PIMD Orientational ITACF of C Axis

The behaviour of these ITACFs is similar to that of a free rotor, although the results do not exactly match up (they are offset by a slight shift in decorrelation amplitude). This may be due to non-rigid body effects that are unaccounted for in the rigid rotor model used when calculating the exact orientational ITACFs. This could also be attributed to incomplete sampling of the PIMD simulations, due to the sampling problem aforementioned. Due to the large errors in the correlation functions and the uncertain structure of the energy levels, it proved to be implausible to curve-fit the obtained correlation functions to the form of the exact ITACF in order to extract exact energy levels.

Chapter 4

Exact Diagonalization

In addition to the path integral simulations that were conducted, exact diagonalization code was developed in order to gain direct access to the systems energy eigenvalues. This way, level splitting can be directly observed by looking at the energy levels themselves. Additionally, access to the energy-levels and wavefunctions opens up pathways through which much more can be learned about the system, as well as provide us with a standard to test PIMD results against.

Code was developed in python in order to perform the exact diagonalization, and is detailed in the remainder of this chapter.

4.1 Hamiltonian – Setting the Stage

In order to obtain energy values through exact diagonalization, we must first describe the Hamiltonian of the system. We begin by writing the general Hamiltonian which is just a sum of the kinetic and potential energy:

$$\hat{H} = \hat{T} + \hat{V} \tag{4.1}$$

Here, \hat{T} is the kinetic energy operator ($\frac{\hat{p}^2}{2m}$), and \hat{V} is the potential energy operator

(this contains information about interactions). In our calculation we work within the rigid rotor approximation, meaning that the molecular vibrational modes are approximated as uncoupled from the rest of the Hamiltonian due to the difference in magnitude of frequencies and as such do not affect the low lying energy states that we are interested in. Thus, since the molecular vibrations occur so fast, the molecule is treated as rigid, and the remaining kinetic energy terms include just rotational and translational energy. As with the PIMD simulations, the buckyball cage is treated as a rigid object whose contribution to the Hamiltonian becomes the external potential that the water feels.

$$\hat{H} = \hat{T}_{trans} + \hat{T}_{rot} + \hat{V}_{ext} \quad (4.2)$$

Substituting the known operators, and recognizing that \hat{V}_{ext} is the sum of the Lennard-Jones interaction potential between each carbon atom from the cage and each atom in the water molecule, this can be explicitly written as:

$$\hat{H} = \frac{\hat{p}^2}{2m} + \frac{J_a^2}{2I_a} + \frac{J_b^2}{2I_b} + \frac{J_c^2}{2I_c} + \sum_{n=1}^3 \sum_{c=1}^{60} 4\epsilon \left[\left(\frac{\sigma}{r} \right)^{12} - \left(\frac{\sigma}{r} \right)^6 \right] \quad (4.3)$$

4.2 Calculating the Potential

In order to calculate the matrix elements $\langle klm | \langle JKM | \hat{V} | J'K'M' \rangle | k'l'm' \rangle$ we must first calculate the potential, defined previously as the sum of Lennard-Jones interactions on our six dimensional grid. This was accomplished by first defining a grid for the center of mass position of the water in spherical coordinates (r, θ, ϕ) . At each point in this grid, another grid was defined in terms of the three Euler angles (θ, ϕ, χ) representing the orientation of the water. In order to incorporate this orientation information, the water was rotated from the molecular fixed frame (MFF) into the space fixed frame (SFF) using the rotation matrix:

$$R = \begin{pmatrix} \cos \phi \cos \theta \cos \chi - \sin \phi \sin \chi & -\cos \phi \cos \theta \sin \chi - \sin \phi \cos \chi & \cos \phi \sin \theta \\ \sin \phi \cos \theta \cos \chi + \cos \phi \sin \chi & -\sin \phi \cos \theta \sin \chi + \cos \phi \cos \chi & \sin \phi \sin \theta \\ -\sin \theta \cos \chi & \sin \theta \sin \chi & \cos \theta \end{pmatrix}$$

By rotating the MFF position vector of each atom of the molecule by this matrix, the new coordinates for each atom are obtained for a given set of Euler angles. After the coordinates of the atoms have been determined for a given center of mass and orientation of the water molecule, the potential is calculated by performing the sum over Lennard-Jones between each atom in the water and each carbon in the buckyball. The coordinates for the carbon atoms are read in from a data file, and since this is a very general procedure it is very easy to exchange the external potential due to a buckyball in favour of an external potential with a different geometry and/or interaction strength e.g, argon matrix, C_{70} , etc...

Following this procedure, we have obtained the potential in terms of the six degrees of freedom $V(r, \theta_p, \phi_p, \theta_o, \phi_o, \chi)$ where p and o denote position and orientation, respectively.

4.3 Choosing a Basis

To solve this Hamiltonian, we require a complete basis that overlaps with each degree of freedom defined by the operators in our Hamiltonian. The translational part has three positional coordinates, the rotational part since water is an asymmetric top has three Euler angles specifying orientation, and the external potential couples all six of these degrees of freedom. Since the external potential appears to be strongly harmonic, we choose to work in a 3D isotropic harmonic oscillator in spherical coordinates ($|\psi_{klm}\rangle$) for the translational part, and the familiar eigenfunctions of a freely rotating symmetric top ($|\psi_{JKM}\rangle$) for the rotational part. The full basis may be represented as $|klm\rangle \otimes |JKM\rangle$

4.3.1 $\langle JKM|$

In order to calculate matrix elements, the coordinate representation of the $\langle JKM|$ basis needs to be known:

$$\langle JKM|\theta_o, \phi_o, \chi\rangle = \sqrt{\frac{2J+1}{8\pi^2}} D_{MK}^J(\theta_o, \phi_o, \chi) \quad (4.4)$$

where $D_{MK}^J(\theta_o, \phi_o, \chi)$ is a Wigner-D matrix, defined as:

$$D_{MK}^J(\theta_o, \phi_o, \chi) = e^{-iM\phi} d_{MK}^J(\theta) e^{-iK\chi} \quad (4.5)$$

and

$$\begin{aligned} d_{MK}^J(\theta) &= \sqrt{(J+M)!(J-M)!(J+M')!(J-M')!} \\ &\times \sum_{\nu} \frac{(-1)^{\nu}}{(J-M'-\nu)!(J+M-\nu)!(\nu+M'-M)!\nu!} \\ &\times \left[\cos\left(\frac{\theta}{2}\right) \right]^{2J+M-M'-2\nu} \left[-\sin\left(\frac{\theta}{2}\right) \right]^{M'-M+2\nu} \end{aligned}$$

The sum over ν is for all positive integer factorial arguments.

4.3.2 $\langle klm|$

The coordinate representation of the klm basis is separable into a radial part and an angular part.

$$\langle klm|r, \theta_p, \phi_p\rangle = N_{kl} r^l e^{-\nu r^2} L_k^{l+\frac{1}{2}}(2\nu r^2) Y_{lm}(\theta_p, \phi_p) \quad (4.6)$$

Here, ν represents $\frac{m\omega}{2\hbar}$, where m is mass and ω is natural frequency, and N_{kl} is a

normalization constant defined by:

$$N_{kl} = \sqrt{\sqrt{\frac{2\nu^3}{\pi} \frac{2^{k+2l+3} k! \nu^l}{(2k+2l+1)!!}} \quad (4.7)$$

$L_k^{l+\frac{1}{2}}(2\nu r^2)$ represents a generalized Laguerre polynomial, and $Y_{lm}(\theta, \phi)$ is a spherical harmonic.

4.4 Matrix Elements

In order to determine the eigenvalues of this Hamiltonian, we must calculate the matrix elements in the chosen basis.

The translational part of the Hamiltonian only acts on the $|klm\rangle$ basis, and is diagonal in $|JKM\rangle$, whereas the rotational part of the Hamiltonian acts only upon the $|JKM\rangle$ and is diagonal in $|klm\rangle$. The external potential due to the cage couples to both the $|klm\rangle$ and the $|JKM\rangle$ which is why this problem is non-trivial.

$$\begin{aligned} & \langle klm | \langle JKM | \hat{H} | J'K'M' \rangle | k'l'm' \rangle \\ &= \langle klm | \langle JKM | \hat{T}_{trans} + \hat{T}_{rot} + \hat{V}_{ext} | J'K'M' \rangle | k'l'm' \rangle \\ &= \langle klm | \langle JKM | \hat{T}_{trans} | J'K'M' \rangle | k'l'm' \rangle + \langle klm | \langle JKM | \hat{T}_{rot} | J'K'M' \rangle | k'l'm' \rangle \\ &+ \langle klm | \langle JKM | \hat{V}_{ext} | J'K'M' \rangle | k'l'm' \rangle \\ &= \langle klm | \frac{\hat{p}^2}{2m} | k'l'm' \rangle \delta_{J,J'} \delta_{K,K'} \delta_{M,M'} + \langle JKM | \hat{T}_{rot} | J'K'M' \rangle \delta_{k,k'} \delta_{l,l'} \delta_{m,m'} \\ &+ \langle klm | \langle JKM | \hat{V}_{ext} | J'K'M' \rangle | k'l'm' \rangle \end{aligned}$$

In order to solve the translational part, we add and subtract $\frac{1}{2}m\omega^2 r^2$ from the Hamiltonian in order to obtain the 3D isotropic h.o. and an extra r^2 term. Since the 3D isotropic

h.o. is diagonal in the chosen basis, the kinetic energy is all taken care of in diagonal terms. All that remains is a quadrature in the r-grid. The rotational part of the Hamiltonian is the same for the free water case. The Hamiltonian becomes:

$$\begin{aligned}
& \langle klm | \frac{\hat{p}^2}{2m} \pm \frac{1}{2} m \omega^2 r^2 | k'l'm' \rangle \delta_{J,J'} \delta_{K,K'} \delta_{M,M'} + \langle JKM | \hat{T}_{rot} | J'K'M' \rangle \delta_{k,k'} \delta_{l,l'} \delta_{m,m'} \\
& + \langle klm | \langle JKM | \hat{V}_{ext} | J'K'M' \rangle | k'l'm' \rangle \\
& = \langle klm | \hat{H}_{qho} | k'l'm' \rangle \delta_{J,J'} \delta_{K,K'} \delta_{M,M'} - \langle klm | \frac{1}{2} m \omega^2 r^2 | k'l'm' \rangle \delta_{J,J'} \delta_{K,K'} \delta_{M,M'} \\
& + \langle JKM | \hat{T}_{rot} | J'K'M' \rangle \delta_{k,k'} \delta_{l,l'} \delta_{m,m'} + \langle klm | \langle JKM | \hat{V}_{ext} | J'K'M' \rangle | k'l'm' \rangle \\
& = \hbar \omega \left(2k + l + \frac{3}{2} \right) \delta_{J,J'} \delta_{K,K'} \delta_{M,M'} \delta_{k,k'} \delta_{l,l'} \delta_{m,m'} - \langle klm | \frac{1}{2} m \omega^2 r^2 | k'l'm' \rangle \delta_{J,J'} \delta_{K,K'} \delta_{M,M'} \\
& + \langle JKM | \hat{T}_{rot} | J'K'M' \rangle \delta_{k,k'} \delta_{l,l'} \delta_{m,m'} + \langle klm | \langle JKM | \hat{V}_{ext} | J'K'M' \rangle | k'l'm' \rangle
\end{aligned}$$

The remaining terms, $\langle klm | \frac{1}{2} m \omega^2 r^2 | k'l'm' \rangle$ and $\langle klm | \langle JKM | \hat{V}_{ext} | J'K'M' \rangle | k'l'm' \rangle$ are calculated using numerical integration.

4.5 Code Testing and Preliminary Results

In order to test the code for reliability, the following measures were taken. The basis that were used for the quadrature calculations were tested to be orthonormal. In order to accomplish this, the interaction potential was set to 1 in the potential matrix element calculations. This results in a potential matrix that is equal to the identity since, with a potential interaction of 1, the matrix element is just the inner product of two basis functions (a Kronecker delta).

Additionally, the Hamiltonian comprised of just the 3D isotropic h.o. and the asymmetric top was looked at. Since there is no term coupling the JKM or lmn basis functions, the resulting diagonalization shows this. The eigenvalues are just the combination of the 3D

isotropic h.o. and the asymmetric top rotational functions. The eigenvalues of this is shown for the case where $J_{\max} = 1$ and $N_{\max} = 2$.

Table 4.1: Calculated Energy Levels for: A- No potential interaction term (Only 3D Isotropic H.O. and Asymmetric Rotor); B- Full Hamiltonian

state	A		B	
	energy (cm-1)	Δ energy (cm-1)	energy (cm-1)	Δ energy (cm-1)
0	257.64	0	-1829.19	0
1	281.44	23.8	-1805.62	24
2	281.44	23.8	-1805.21	24
3	281.44	23.8	-1804.89	24
4	294.8	37.16	-1791.70	37
5	294.8	37.16	-1791.52	38
6	294.8	37.16	-1791.52	38
7	300.03	42.39	-1787.10	42
8	300.03	42.39	-1786.57	43
9	300.03	42.39	-1786.27	43
10	327.78	70.13	-1758.89	70
11	327.78	70.13	-1758.46	71
12	327.78	70.13	-1758.45	71
13	327.78	70.13	-1758.35	71
14	327.78	70.13	-1750.04	79
15	337.17	79.53	-1749.39	80
16	337.17	79.53	-1749.25	80
17	337.17	79.53	-1748.93	80
18	337.17	79.53	-1748.88	80
19	337.17	79.53	-1748.88	80
20	352.85	95.21	-1734.48	95
21	352.85	95.21	-1733.28	96
22	352.85	95.21	-1733.28	96
23	352.85	95.21	-1732.84	96
24	352.85	95.21	-1701.29	128

Here in column A eigenvalues are the eigenvalues of the 3D isotropic h.o. simply added to the eigenvalues of the rotational Hamiltonian. The zero point energy of the 3D Isotropic h.o. is at 257.64 cm^{-1} . Column B shows the calculated eigenvalues for the full Hamiltonian of the system. These results are still preliminary as the potential interaction matrix elements are not yet converged, with the grid size, and the ground state energy is not yet converged variationally. This result is for a grid size of (70,50,50,24,25,25) corresponding to $(r, \theta_p, \phi_p, \theta_o, \phi_o, \chi)$, and a J_{\max} of 2, N_{\max} of 3.

The energy levels can be tested against the results recently published by Felker and Bačić²⁸ in a study where they also investigated the 6D calculations of the translation-rotation eigenstates of the $H_2O@C_{60}$, as we can match parameters and compare the resulting eigenvalues. Felker and Bačić used the exact same L-J potential discussed previously to take into account the water-buckyball interaction, and used a water geometry defined by the molecular fixed coordinates (x,y,z) in angstroms:

O: (0.0,0.0,-0.06563807)

H1: (0.7575,0.0,0.52086193)

H2: (-0.7575,0.0,0.52086193)

with rotational constants in cm^{-1} :

A: 27.877

B: 14.512

C: 9.285

and a total mass of 18.01056 amu. The coordinates for the carbon cage can be found in the supplementary material for the publication.²⁸

It was discovered that the ground state energy of the system was located at $E_0 = -1987.57 cm^{-1}$, with the next excited state being triply degenerate (no splitting) at $23.74 cm^{-1}$ above the ground state. This indicates that a single cage is not enough to split the rotational levels.

It is clear that our results are unconverged as our ground state energy is still over $100 cm^{-1}$ off from the published data. This means that many more basis functions will be required, as well as a larger grid size. Even though the absolute energy may be unconverged, the difference in energy between a certain state and the ground state still seem to be very close

to one another.

4.6 Outlook

This code is finished development, and is ready to be used. Currently being applied to the endohedral water system, the results are incomplete as the energy values have yet to converge with respect to the coordinate grid size $(r, \theta_p, \phi_p, \theta_o, \phi_o, \chi)$ and basis size. Since one buckyball does not split the rotational levels of water by itself, the effect of the next nearest C_{60} neighbours will be looked at. The eigenvalues of the low-lying states can be compared for single cage, an H-phase cage, and a P-phase cage,²⁹ where these phases refer to the orientation of the buckyballs in the crystal lattice. Once the H- or P- phase is taken into account, it is expected that we find a slight lifting of the degeneracy, due to the reduced symmetry of the crystal versus the buckyball itself.

The code may easily be utilized in a number of other systems, and should be a powerful tool for continuing work on this and other similar systems.

Chapter 5

Conclusion

In this work, tools were developed and utilized in order to investigate the $H_2O@C_{60}$ and similar systems. The tools were developed with the goal of modelling these systems accurately in order to gain a better understanding of the quantum phenomena that are present in experiments. This includes level splitting in the rotational *ortho* ground state, *ortho-para* conversion, and long-range dipole interactions.

The first method utilized in pursuit of understanding this system was path integral molecular dynamics simulations. Imaginary time autocorrelation functions were examined for the orientation of the water, in order to see if the splitting could be captured through this method but to no success due to the difficulty of trying to curve the proper form of the correlation functions (sum of exponentials). These simulations were conducted for a system consisting of only a single water molecule in a single buckyball and several thermodynamic properties were obtained including various distributions as well as rotational imaginary time autocorrelation functions. Although, it is now believed that the splitting is not due to one cage, but due to a many-body effect from both the crystalline structure of the buckyballs, as well as from the dipolar interactions with the other waters encapsulated within the surrounding buckyballs.

In addition to the path integral simulations, exact diagonalization code was developed

in order to variationally calculate the energy levels of the water directly. The code that was written is very general and can easily be applied to multiple other systems, mainly by interchanging the guest/host molecule.

5.1 Future Work

There is still much work to be done for the $H_2O@C_{60}$ system. Described in this work, tools have been developed in order to study a single water in a single cage, but may certainly be extended in a wide number of ways to aid in future studies of this or related systems. An immediate step for future work would be to complete converging results using the exact diagonalization code that was developed on the single water, single cage system, and extend it to larger systems. In order to converge results, the grid size in the coordinate representation as well as the basis size must all be large enough. Once this is complete, there are many calculations that may immediately be run that are related to the thermodynamic properties of the system. Various distributions again, and exact orientational imaginary time autocorrelation functions for the caged water may be computed, and then subsequently compared to the PIMD results.

Another direction for future work is to expand the existing code in order to probe many-body effects. This is important as the interesting quantum phenomena are believed to be due to many-body effects. It is upon understanding and utilizing these many-body quantum effects that may allow us to find real applications for this material. In order to include many-body effects, the simulation or calculation size may be modified by including n -repeating units of the $H_2O@C_{60}$ complex in a crystalline structure. Although both simulations and calculations may suffer from too-long run times or not enough memory, there may be clever ways to incorporate information from both exact diagonalization techniques as well as path integral simulations.

An additional direction of future work is to vary host/guest molecules, meaning exchanging either the water with another guest, such as the $HF@C_{60}$ molecule that was

recently synthesized.³⁰ In principal, the code that was developed is immediately ready to tackle this system, provided that a sufficient HF - C₆₀ potential is available. Different systems may behave differently, and other interesting effects may become evident. It is a simple task to extend the existing work to include alternative host/guest molecules. All that is required is for the host molecule geometry data file to be modified and the interaction parameters updated for the simulations or the calculations, as the code is very general.

Lastly, modifying the exact diagonalization code to also capture the *ortho-para* spin conversion is another interesting direction for future work that can be built off of the tools described in this work. In order to capture spin-conversion, the Hamiltonian of the exact code must be modified. The basis will have to be modified as well in order to include nuclear spin in the Hilbert space, thus adding a dimension and forcing slower calculation times.

References

- [1] L. Ulivi, *et al.*, *Phys. Rev. B* **76**, 161401 (2007).
- [2] L. Ulivi, M. Celli, A. Giannasi, A. J. Ramirez-Cuesta, M. Zoppi, *J. Phys.: Condens. Matter* **20**, 104242 (2008).
- [3] M. Xu, F. Sebastianelli, Z. Bačić, R. Lawler, N. J. Turro, *J. Chem. Phys.* **129**, (2008).
- [4] Y. Li, *et al.*, *J. Phys. Chem. Lett.* **3**, 1165 (2012).
- [5] K. Kurotobi, Y. Murata, *Science* **333**, 613 (2011).
- [6] A. Krachmalnicoff, M. H. Levitt, R. J. Whitby, *Chem. Commun.* **50**, 13037 (2014).
- [7] M. Concistrè, *et al.*, *Phil. Trans. R. Soc. A* **371** (2013).
- [8] J. Y.-C. Chen, *et al.*, *Phil. Trans. R. Soc. A* **371** (2013).
- [9] C. Beduz, *et al.*, *PNAS* **109**, 12894 (2012).
- [10] S. Mamone, *et al.*, *J. Chem. Phys.* **140**, (2014).
- [11] D. S. Sabirov, *J. Phys. Chem. C* **117**, 1178 (2013).
- [12] B. Ensing, F. Costanzo, P. L. Silvestrelli, *J. Phys. Chem. A* **116**, 12184 (2012).
- [13] B. Xu, X. Chen, *Phys. Rev. Lett.* **110**, 156103 (2013).
- [14] A. B. Farimani, Y. Wu, N. R. Aluru, *Phys. Chem. Chem. Phys.* **15**, 17993 (2013).

- [15] D. Bucher, *Chem. Phys. L.* **534**, 38 (2012).
- [16] C. Ramachandran, N. Sathyamurthy, *Chem. Phys. L.* **410**, 348 (2005).
- [17] K. Yagi, D. Watanabe, *Int. J. Quant. Chem.* **109**, 2080 (2009).
- [18] A. L. Balch, *Science* **333**, 531 (2011).
- [19] S. Aoyagi, *et al.*, *Chem. Commun.* **50**, 524 (2014).
- [20] R. Zhang, M. Murata, A. Wakamiya, Y. Murata, *Chem. Lett.* **42**, 879 (2013).
- [21] M. Trainer, *Eur. J. Phys.* **21**, 459 (2000).
- [22] R. Zare, *Angular Momentum: Understanding Spatial Aspects in Chemistry and Physics* (Wiley Inter-Science, 1988).
- [23] R. Feynman, *Statistical Mechanics: A Set Of Lectures*, Advanced Book Classics (Westview Press, 1998).
- [24] M. F. Herman, E. J. Bruskin, B. J. Berne, *J. Chem. Phys.* **76**, 5150 (1982).
- [25] K. Hinsien, *J. Comput. Chem.* **21**, 79 (2000).
- [26] M. Ceriotti, M. Parrinello, T. E. Markland, D. E. Manolopoulos, *J. Chem. Phys.* **133**, (2010).
- [27] G. Bussi, M. Parrinello, *Phys. Rev. E* **75**, 056707 (2007).
- [28] P. M. Felker, Z. Bačić, *The Journal of Chemical Physics* **144** (2016).
- [29] M. Álvarez Murga, J. Hodeau, *Carbon* **82**, 381 (2015).
- [30] A. Krachmalnicoff, *et al.*, *Nat Chem* **advance online publication**.

Appendix A

Exact ITACF using Spherical Coordinates

In order to gain insight on the rotational eigenstates of a water molecule (free and confined), we may study the orientational autocorrelation function. For a free water we may calculate this exactly, through diagonalization of the asymmetric top hamiltonian in the symmetric top basis ($|JKM\rangle$), and for the confined case we may measure these correlation functions directly along the path in a PIMD/PIMC simulation.

In order to calculate the exact orientational ITACFs, it is required of us to write the orientation vectors of the water in the space fixed frame so that we can solve the matrix elements in the $|JKM\rangle$ basis.

In the molecular fixed frame, the orientation vectors can be written simply as:

$$e^x = \begin{pmatrix} 1 \\ 0 \\ 0 \end{pmatrix}, e^y = \begin{pmatrix} 0 \\ 1 \\ 0 \end{pmatrix}, e^z = \begin{pmatrix} 0 \\ 0 \\ 1 \end{pmatrix}$$

where e^x corresponds to the molecular a axis, e^y is the c axis, and e^z is the b axis.

In order to determine these vectors in the space fixed frame (under some arbitrary rotation), we need to multiply the vectors with the rotation matrix:

$$R = \begin{pmatrix} \cos \phi \cos \theta \cos \chi - \sin \phi \sin \chi & -\cos \phi \cos \theta \sin \chi - \sin \phi \cos \chi & \cos \phi \sin \theta \\ \sin \phi \cos \theta \cos \chi + \cos \phi \sin \chi & -\sin \phi \cos \theta \sin \chi + \cos \phi \cos \chi & \sin \phi \sin \theta \\ -\sin \theta \cos \chi & \sin \theta \sin \chi & \cos \theta \end{pmatrix}$$

Thus, we can write our SFF orientation vectors as $n \times R$:

$$\begin{aligned} V^x &= e^x \times R \\ &= \begin{pmatrix} 1 \\ 0 \\ 0 \end{pmatrix} \times \begin{pmatrix} \cos \phi \cos \theta \cos \chi - \sin \phi \sin \chi & -\cos \phi \cos \theta \sin \chi - \sin \phi \cos \chi & \cos \phi \sin \theta \\ \sin \phi \cos \theta \cos \chi + \cos \phi \sin \chi & -\sin \phi \cos \theta \sin \chi + \cos \phi \cos \chi & \sin \phi \sin \theta \\ -\sin \theta \cos \chi & \sin \theta \sin \chi & \cos \theta \end{pmatrix} \\ &= \begin{pmatrix} \cos \phi \cos \theta \cos \chi - \sin \phi \sin \chi \\ \sin \phi \cos \theta \cos \chi + \cos \phi \sin \chi \\ -\sin \theta \cos \chi \end{pmatrix} \end{aligned}$$

$$\begin{aligned} V^y &= e^y \times R \\ &= \begin{pmatrix} 0 \\ 1 \\ 0 \end{pmatrix} \times \begin{pmatrix} \cos \phi \cos \theta \cos \chi - \sin \phi \sin \chi & -\cos \phi \cos \theta \sin \chi - \sin \phi \cos \chi & \cos \phi \sin \theta \\ \sin \phi \cos \theta \cos \chi + \cos \phi \sin \chi & -\sin \phi \cos \theta \sin \chi + \cos \phi \cos \chi & \sin \phi \sin \theta \\ -\sin \theta \cos \chi & \sin \theta \sin \chi & \cos \theta \end{pmatrix} \\ &= \begin{pmatrix} -\cos \phi \cos \theta \sin \chi - \sin \phi \cos \chi \\ -\sin \phi \cos \theta \sin \chi + \cos \phi \cos \chi \\ \sin \theta \sin \chi \end{pmatrix} \end{aligned}$$

and finally

$$\begin{aligned}
V^z &= e^z \times R \\
&= \begin{pmatrix} 0 \\ 0 \\ 1 \end{pmatrix} \times \begin{pmatrix} \cos \phi \cos \theta \cos \chi - \sin \phi \sin \chi & -\cos \phi \cos \theta \sin \chi - \sin \phi \cos \chi & \cos \phi \sin \theta \\ \sin \phi \cos \theta \cos \chi + \cos \phi \sin \chi & -\sin \phi \cos \theta \sin \chi + \cos \phi \cos \chi & \sin \phi \sin \theta \\ -\sin \theta \cos \chi & \sin \theta \sin \chi & \cos \theta \end{pmatrix} \\
&= \begin{pmatrix} \cos \phi \sin \theta \\ \sin \phi \sin \theta \\ \cos \theta \end{pmatrix}
\end{aligned}$$

In order to solve the matrix elements of $V^{x,y,z}$ in the JKM basis, it would require the use of quadratures although we may find that if we define vectors in terms of the spherical basis, we can have analytical solutions to the integrals. The spherical basis is defined as:

$$\begin{aligned}
e^+ &= -\frac{1}{\sqrt{2}}e^x - \frac{i}{\sqrt{2}}e^y \\
e^- &= \frac{1}{\sqrt{2}}e^x - \frac{i}{\sqrt{2}}e^y \\
e^0 &= e^z
\end{aligned}$$

Therefore, in the SFF, the spherical basis vectors of the water are defined as:

$$\begin{aligned}
V^+ &= -\frac{1}{\sqrt{2}}(X + iY) \\
&= -\frac{1}{\sqrt{2}} \begin{pmatrix} \cos \phi \cos \theta \cos \chi - \sin \phi \sin \chi - i \cos \phi \cos \theta \sin \chi - i \sin \phi \cos \chi \\ \sin \phi \cos \theta \cos \chi + \cos \phi \sin \chi - i \sin \phi \cos \theta \sin \chi + i \cos \phi \cos \chi \\ -\sin \theta \cos \chi + i \sin \theta \sin \chi \end{pmatrix}
\end{aligned}$$

$$\begin{aligned}
V^- &= \frac{1}{\sqrt{2}}(X - iY) \\
&= -\frac{1}{\sqrt{2}} \begin{pmatrix} \cos \phi \cos \theta \cos \chi - \sin \phi \sin \chi + i \cos \phi \cos \theta \sin \chi + i \sin \phi \cos \chi \\ \sin \phi \cos \theta \cos \chi + \cos \phi \sin \chi + i \sin \phi \cos \theta \sin \chi - i \cos \phi \cos \chi \\ -\sin \theta \cos \chi - i \sin \theta \sin \chi \end{pmatrix}
\end{aligned}$$

$$\begin{aligned}
V^0 &= Z \\
&= \begin{pmatrix} \cos \phi \sin \theta \\ \sin \phi \sin \theta \\ \cos \theta \end{pmatrix}
\end{aligned}$$

These spherical basis vectors are still represented in the cartesian basis though, and one further transformation to the spherical basis is required in order to find the useful symmetries.

The coordinates transform as the complex conjugate of the basis ie.

$$\begin{aligned}
V_+ &= -\frac{1}{\sqrt{2}}V_x + \frac{i}{\sqrt{2}}V_y \\
V_- &= \frac{1}{\sqrt{2}}V_x + \frac{i}{\sqrt{2}}V_y \\
V_0 &= V_z
\end{aligned}$$

Looking at the V^+ vector, we thus see that in terms of spherical components:

$$\begin{aligned}
V_+^+ &= -\frac{1}{\sqrt{2}}(V_x^+ - iV_y^+) \\
&= -\frac{1}{\sqrt{2}}\left[-\frac{1}{\sqrt{2}}(\cos\phi\cos\theta\cos\chi - \sin\phi\sin\chi - i\cos\phi\cos\theta\sin\chi - i\sin\phi\cos\chi\right. \\
&\quad \left.- i(\sin\phi\cos\theta\cos\chi + \cos\phi\sin\chi - i\sin\phi\cos\theta\sin\chi + i\cos\phi\cos\chi))\right] \\
&= \frac{1}{2}[\cos\phi\cos\theta\cos\chi - \sin\phi\sin\chi - i\cos\phi\cos\theta\sin\chi - i\sin\phi\cos\chi \\
&\quad - i\sin\phi\cos\theta\cos\chi - i\cos\phi\sin\chi - \sin\phi\cos\theta\sin\chi + \cos\phi\cos\chi] \\
&= \frac{1}{2}[\cos\phi\cos\theta(\cos\chi - i\sin\chi) - \sin\phi(\sin\chi + i\cos\chi) - \cos\phi(i\sin\chi - \cos\chi) - \sin\phi\cos\theta(i\cos\chi + \sin\chi)] \\
&= \frac{1}{2}[\cos\phi\cos\theta e^{-i\chi} - i\sin\phi(\cos\chi - i\sin\chi) + \cos\phi(\cos\chi - i\sin\chi) - i\sin\phi\cos\theta(\cos\chi - i\sin\chi)] \\
&= \frac{1}{2}[\cos\phi\cos\theta e^{-i\chi} - i\sin\phi e^{-i\chi} + \cos\phi e^{-i\chi} - i\sin\phi\cos\theta e^{-i\chi}] \\
&= \frac{e^{-i\chi}}{2}[\cos\phi\cos\theta + \cos\phi - i\sin\phi - i\sin\phi\cos\theta] \\
&= \frac{1}{2}e^{-i\chi}e^{-i\phi}(\cos\theta + 1) \\
&= D_{11}^1
\end{aligned}$$

$$\begin{aligned}
V_-^+ &= \frac{1}{\sqrt{2}}(V_x^+ + iV_y^+) \\
&= \frac{1}{\sqrt{2}}\left[-\frac{1}{\sqrt{2}}(\cos\phi\cos\theta\cos\chi - \sin\phi\sin\chi - i\cos\phi\cos\theta\sin\chi - i\sin\phi\cos\chi\right. \\
&\quad \left.+ i(\sin\phi\cos\theta\cos\chi + \cos\phi\sin\chi - i\sin\phi\cos\theta\sin\chi + i\cos\phi\cos\chi))\right] \\
&= -\frac{1}{2}[\cos\phi\cos\theta\cos\chi - \sin\phi\sin\chi - i\cos\phi\cos\theta\sin\chi - i\sin\phi\cos\chi \\
&\quad + i\sin\phi\cos\theta\cos\chi + i\cos\phi\sin\chi + \sin\phi\cos\theta\sin\chi - \cos\phi\cos\chi] \\
&= -\frac{1}{2}[\cos\phi\cos\theta(\cos\chi - i\sin\chi) - i\sin\phi(\cos\chi - i\sin\chi) + i\sin\chi\cos\theta(\cos\chi - \sin\chi) - \cos\phi(\cos\chi - i\sin\chi)] \\
&= -\frac{1}{2}e^{-i\chi}[\cos\phi\cos\theta - i\sin\phi + i\sin\chi\cos\theta - \cos\theta] \\
&= -\frac{1}{2}e^{-i\chi}[\cos\theta e^{i\phi} - e^{i\phi}] \\
&= \frac{1}{2}e^{-i\chi}e^{i\phi}[1 - \cos\theta] \\
&= D_{-11}^1
\end{aligned}$$

$$\begin{aligned}
V_0^+ &= V_z^+ \\
&= \frac{1}{\sqrt{2}} \sin \theta \cos \chi - \frac{1}{\sqrt{2}} i \sin \theta \sin \chi \\
&= \frac{1}{\sqrt{2}} \sin \theta (\cos \chi - i \sin \chi) \\
&= \frac{1}{\sqrt{2}} \sin \theta e^{-i\chi} \\
&= D_{01}^1
\end{aligned}$$

For the V^- vector, we find:

$$\begin{aligned}
V_+^- &= -\frac{1}{\sqrt{2}}(V_x^- - iV_y^+) \\
&= -\frac{1}{2}[(V_x^x - iV_x^y) - i(V_y^x - iV_y^y)] \\
&= -\frac{1}{2}[\cos \phi \cos \theta \cos \chi - \sin \phi \sin \chi + i \cos \phi \cos \theta \sin \chi + i \sin \phi \cos \chi \\
&\quad - i \sin \phi \cos \theta \cos \chi - i \cos \phi \sin \chi + \sin \phi \cos \theta \sin \chi - \cos \phi \cos \chi] \\
&= -\frac{1}{2}[\cos \phi \cos \theta (\cos \chi + i \sin \chi) + i \sin \phi (\cos \chi + i \sin \chi) \\
&\quad - i \sin \phi \cos \theta (\cos \chi + i \sin \chi) - \cos \phi (\cos \chi + i \sin \chi)] \\
&= -\frac{1}{2}e^{i\chi}[\cos \phi \cos \theta + i \sin \phi - i \sin \phi \cos \theta - \cos \phi] \\
&= -\frac{1}{2}e^{i\chi}[\cos \theta (\cos \phi - i \sin \phi) - (\cos \phi - i \sin \phi)] \\
&= -\frac{1}{2}e^{i\chi}e^{-i\phi}[1 - \cos \theta] \\
&= D_{1-1}^1
\end{aligned}$$

$$\begin{aligned}
V_-^- &= \frac{1}{\sqrt{2}}(V_x^- + iV_y^-) \\
&= \frac{1}{2}[(V_x^x - iV_x^y) + i(V_y^x + iV_y^y)] \\
&= \frac{1}{2}[\cos \phi \cos \theta \cos \chi - \sin \phi \sin \chi + i \cos \phi \cos \theta \sin \chi + i \sin \phi \cos \chi \\
&\quad + i \sin \phi \cos \theta \cos \chi + i \cos \phi \sin \chi - \sin \phi \cos \theta \sin \chi + \cos \phi \cos \chi] \\
&= \frac{1}{2}[\cos \phi \cos \theta (\cos \chi + i \sin \chi) + i \sin \phi (\cos \chi + i \sin \chi) \\
&\quad + i \sin \phi \cos \theta (\cos \chi + i \sin \chi) + \cos \phi (\cos \chi + i \sin \chi)] \\
&= \frac{1}{2}e^{i\chi}[\cos \phi \cos \theta + i \sin \phi + i \sin \phi \cos \theta + \cos \phi] \\
&= \frac{1}{2}e^{i\chi}[\cos \theta (\cos \phi + i \sin \phi) + (\cos \phi + i \sin \phi)] \\
&= \frac{1}{2}e^{i\chi}e^{i\phi}[1 + \cos \theta] \\
&= D_{-1-1}^1
\end{aligned}$$

$$\begin{aligned}
V_0^- &= V_z^- \\
&= \frac{1}{\sqrt{2}}(V_z^x - iV_z^y) \\
&= -\frac{1}{\sqrt{2}}(\sin \theta \cos \chi + i \sin \theta \sin \chi) \\
&= -\frac{1}{\sqrt{2}}\sin \theta (\cos \chi + i \sin \chi) \\
&= -\frac{1}{\sqrt{2}}\sin \theta e^{i\chi} \\
&= D_{0-1}^1
\end{aligned}$$

And last for the V^0 vector, we find:

$$\begin{aligned}
V_+^0 &= -\frac{1}{\sqrt{2}}(V_x^0 - iV_y^0) \\
&= -\frac{1}{\sqrt{2}}[\cos \phi \sin \theta - i \sin \phi \sin \theta] \\
&= -\frac{1}{2}[\sin \theta(\cos \phi - i \sin \phi)] \\
&= -\frac{1}{2}e^{-i\phi} \sin \theta \\
&= D_{10}^1
\end{aligned}$$

$$\begin{aligned}
V_-^0 &= \frac{1}{\sqrt{2}}(V_x^0 + iV_y^0) \\
&= \frac{1}{\sqrt{2}}[\cos \phi \sin \theta + i \sin \phi \sin \theta] \\
&= \frac{1}{2}[\sin \theta(\cos \phi + i \sin \phi)] \\
&= \frac{1}{2}e^{i\phi} \sin \theta \\
&= D_{-10}^1
\end{aligned}$$

$$\begin{aligned}
V_0^0 &= V_z^0 \\
&= \cos \theta \\
&= D_{00}^1
\end{aligned}$$

Since what we have obtained is orientation of the water in the molecular frame in terms of the spherical basis completely in terms of Wigner D rotation matrices, we have may complete the integrations of the direction operators in the JKM basis analytically, we just need to write whatever vector in terms of the spherical basis; this will enable us to view the selection rules right away (encoded within the Wigner 3J symbols)

The quantity of interest is $|\langle j\check{k}m|\hat{n}|j'k'm' \rangle|^2$ where \hat{n} is any direction vector. We are interested in when \hat{n} is equal to the any of the molecular axes a,b, or c, as well as the spherical basis vectors.

$$\begin{aligned} & |\langle j\check{k}m|\hat{n}|j'k'm' \rangle|^2 \\ &= \sum_{k_1}^j \sum_{k'_1}^{j'} \sum_{k_2}^j \sum_{k'_2}^{j'} C_{k_1}^{j\check{k}} C_{k'_1}^{j'k'} C_{k_2}^{j\check{k}} C_{k'_2}^{j'k'} \langle jk_1m|\hat{n}|j'k'_1m' \rangle \langle j'k'_2m'|\hat{n}|jk_2m \rangle \end{aligned}$$

if $\hat{n} = V^0 = V^z$ we have

$$\begin{aligned} & \langle jk_1m|V^0|j'k'_1m' \rangle \langle j'k'_2m'|V^0|jk_2m \rangle \\ &= \langle jk_1m|V^0|j'k'_1m' \rangle \langle j'k'_2m'|V^{0*}|jk_2m \rangle \\ &= \langle jk_1m|D_{q0}^1|j'k'_1m' \rangle \langle j'k'_2m'|D_{q0}^{1*}|jk_2m \rangle \\ &= \sum_q (-1)^q \langle jk_1m|D_{q0}^1|j'k'_1m' \rangle \langle j'k'_2m'|D_{-q-0}^1|jk_2m \rangle \\ &= (-1)^{m+m'-k'_1-k_2} (2J+1)(2J'+1) \begin{pmatrix} J & 1 & J' \\ k_1 & 0 & -k'_1 \end{pmatrix} \begin{pmatrix} J' & 1 & J \\ k'_2 & 0 & -k_2 \end{pmatrix} \\ & \sum_q (-1)^q \begin{pmatrix} J & 1 & J' \\ M & q & -M' \end{pmatrix} \begin{pmatrix} J & 1 & J' \\ M' & -q & -M \end{pmatrix} \end{aligned}$$

if $\hat{n} = V^+$ we have

$$\begin{aligned}
& \langle jk_1m|V^+|j'k'_1m' \rangle \langle j'k'_2m'|V^+|jk_2m \rangle \\
& = \langle jk_1m|V^+|j'k'_1m' \rangle \langle j'k'_2m'|V^{+*}|jk_2m \rangle \\
& = \langle jk_1m|D_{q1}^1|j'k'_1m' \rangle \langle j'k'_2m'|D_{q1}^{1*}|jk_2m \rangle \\
& = \sum_q (-1)^{q+1} \langle jk_1m|D_{q1}^1|j'k'_1m' \rangle \langle j'k'_2m'|D_{-q-1}^1|jk_2m \rangle \\
& = (-1)^{m+m'-k'_1-k_2} (2J+1)(2J'+1) \begin{pmatrix} J & 1 & J' \\ k_1 & 1 & -k'_1 \end{pmatrix} \begin{pmatrix} J' & 1 & J \\ k'_2 & -1 & -k_2 \end{pmatrix} \\
& \sum_q (-1)^q \begin{pmatrix} J & 1 & J' \\ M & q & -M' \end{pmatrix} \begin{pmatrix} J & 1 & J' \\ M' & -q & -M \end{pmatrix}
\end{aligned}$$

if $\hat{n} = V^-$ we have

$$\begin{aligned}
& \langle jk_1m|V^-|j'k'_1m' \rangle \langle j'k'_2m'|V^-|jk_2m \rangle \\
& = \langle jk_1m|V^-|j'k'_1m' \rangle \langle j'k'_2m'|V^{-*}|jk_2m \rangle \\
& = \langle jk_1m|D_{q-1}^1|j'k'_1m' \rangle \langle j'k'_2m'|D_{q-1}^{1*}|jk_2m \rangle \\
& = \sum_q (-1)^{q+1} \langle jk_1m|D_{q-1}^1|j'k'_1m' \rangle \langle j'k'_2m'|D_{-q1}^1|jk_2m \rangle \\
& = (-1)^{m+m'-k'_1-k_2} (2J+1)(2J'+1) \begin{pmatrix} J & 1 & J' \\ k_1 & -1 & -k'_1 \end{pmatrix} \begin{pmatrix} J' & 1 & J \\ k'_2 & 1 & -k_2 \end{pmatrix} \\
& \sum_q (-1)^q \begin{pmatrix} J & 1 & J' \\ M & q & -M' \end{pmatrix} \begin{pmatrix} J & 1 & J' \\ M' & -q & -M \end{pmatrix}
\end{aligned}$$

In order to look at the molecular axes (a and c, since b = z and we already solved for that), all we need to do is use the inverse relations of the cartesian basis and spherical basis, ie.

$$\begin{aligned}
e^x &= -\frac{1}{\sqrt{2}}e^+ + \frac{1}{\sqrt{2}}e^- \\
e^y &= \frac{i}{\sqrt{2}}e^+ + \frac{i}{\sqrt{2}}e^- \\
e^z &= e^0
\end{aligned}$$

if $\hat{n} = V^x$ we have

$$\begin{aligned}
&< jk_1m | V^x | j'k'_1m' \rangle \langle j'k'_2m' | V^x | jk_2m \rangle \\
&= \langle jk_1m | V^x | j'k'_1m' \rangle \langle j'k'_2m' | V^{x*} | jk_2m \rangle \\
&= \langle jk_1m | [-\frac{1}{\sqrt{2}}(D_{q1}^1 - D_{q-1}^1)] | j'k'_1m' \rangle \langle j'k'_2m' | [-\frac{1}{\sqrt{2}}(D_{q1}^1 - D_{q-1}^1)]^* | jk_2m \rangle \\
&= \langle jk_1m | [-\frac{1}{\sqrt{2}}(D_{q1}^1 - D_{q-1}^1)] | j'k'_1m' \rangle \langle j'k'_2m' | [-\frac{1}{\sqrt{2}}(D_{q1}^{1*} - D_{q-1}^{1*})] | jk_2m \rangle \\
&= \frac{1}{2} \sum_q (-1)^{q+1} \langle jk_1m | D_{q1}^1 - D_{q-1}^1 | j'k'_1m' \rangle \langle j'k'_2m' | D_{-q-1}^1 - D_{-q1}^1 | jk_2m \rangle \\
&= \frac{1}{2} \sum_q (-1)^{q+1} [\langle jk_1m | D_{q1}^1 | j'k'_1m' \rangle - \langle jk_1m | D_{q-1}^1 | j'k'_1m' \rangle] \\
&[\langle j'k'_2m' | D_{-q-1}^1 | jk_2m \rangle - \langle j'k'_2m' | D_{-q1}^1 | jk_2m \rangle] \\
&= \frac{1}{2} \sum_q (-1)^{q+1} \sqrt{2J+1} \sqrt{2J'+1} (-1)^{m'-k'_1} \left[\begin{pmatrix} J & 1 & J' \\ k_1 & 1 & -k'_1 \end{pmatrix} \begin{pmatrix} J & 1 & J' \\ M & q & -M' \end{pmatrix} \right. \\
&\quad - \begin{pmatrix} J & 1 & J' \\ k_1 & -1 & -k'_1 \end{pmatrix} \begin{pmatrix} J & 1 & J' \\ M & q & -M' \end{pmatrix} \left. \right] \sqrt{2J+1} \sqrt{2J'+1} (-1)^{m-k_2} \left[\begin{pmatrix} J' & 1 & J \\ k'_2 & -1 & -k_2 \end{pmatrix} \begin{pmatrix} J' & 1 & J \\ M' & -q & -M \end{pmatrix} \right. \\
&\quad \left. - \begin{pmatrix} J' & 1 & J \\ k'_2 & 1 & -k_2 \end{pmatrix} \begin{pmatrix} J' & 1 & J \\ M' & -q & -M \end{pmatrix} \right] \\
&= (-1)^{m+m'-k'_1-k_2} \frac{(2J+1)(2J'+1)}{2} \left[\begin{pmatrix} J & 1 & J' \\ k_1 & 1 & -k'_1 \end{pmatrix} - \begin{pmatrix} J & 1 & J' \\ k_1 & -1 & -k'_1 \end{pmatrix} \right] \\
&\quad \left[\begin{pmatrix} J' & 1 & J \\ k'_2 & -1 & -k_2 \end{pmatrix} - \begin{pmatrix} J' & 1 & J \\ k'_2 & 1 & -k_2 \end{pmatrix} \right] \sum_q (-1)^{q+1} \begin{pmatrix} J & 1 & J' \\ M & q & -M' \end{pmatrix} \begin{pmatrix} J' & 1 & J \\ M' & -q & -M \end{pmatrix}
\end{aligned}$$

if $\hat{n} = V^y$ we have

$$\begin{aligned}
& \langle jk_1m|V^y|j'k'_1m' \rangle \langle j'k'_2m'|V^y|jk_2m \rangle \\
&= \langle jk_1m|V^x|j'k'_1m' \rangle \langle j'k'_2m'|V^{y*}|jk_2m \rangle \\
&= \langle jk_1m|[\frac{i}{\sqrt{2}}(D_{q_1}^1 + D_{q-1}^1)]|j'k'_1m' \rangle \langle j'k'_2m'|[\frac{i}{\sqrt{2}}(D_{q_1}^1 + D_{q-1}^1)]^*|jk_2m \rangle \\
&= \langle jk_1m|[\frac{i}{\sqrt{2}}(D_{q_1}^1 + D_{q-1}^1)]|j'k'_1m' \rangle \langle j'k'_2m'|[-\frac{i}{\sqrt{2}}(D_{q_1}^{1*} + D_{q-1}^{1*})]|jk_2m \rangle \\
&= \frac{1}{2} \sum_q (-1)^{q+1} \langle jk_1m|D_{q_1}^1 + D_{q-1}^1|j'k'_1m' \rangle \langle j'k'_2m'|D_{-q-1}^1 + D_{-q_1}^1|jk_2m \rangle \\
&= \frac{1}{2} \sum_q (-1)^{q+1} [\langle jk_1m|D_{q_1}^1|j'k'_1m' \rangle + \langle jk_1m|D_{q-1}^1|j'k'_1m' \rangle] \\
&[\langle j'k'_2m'|D_{-q-1}^1|jk_2m \rangle + \langle j'k'_2m'|D_{-q_1}^1|jk_2m \rangle] \\
&= \frac{1}{2} \sum_q (-1)^{q+1} \sqrt{2J+1} \sqrt{2J'+1} (-1)^{m'-k'_1} \left[\begin{pmatrix} J & 1 & J' \\ k_1 & 1 & -k'_1 \end{pmatrix} \begin{pmatrix} J & 1 & J' \\ M & q & -M' \end{pmatrix} \right. \\
&+ \begin{pmatrix} J & 1 & J' \\ k_1 & -1 & -k'_1 \end{pmatrix} \begin{pmatrix} J & 1 & J' \\ M & q & -M' \end{pmatrix} \left. \right] \sqrt{2J+1} \sqrt{2J'+1} (-1)^{m-k_2} \left[\begin{pmatrix} J' & 1 & J \\ k'_2 & -1 & -k_2 \end{pmatrix} \begin{pmatrix} J' & 1 & J \\ M' & -q & -M \end{pmatrix} \right. \\
&+ \begin{pmatrix} J' & 1 & J \\ k'_2 & 1 & -k_2 \end{pmatrix} \begin{pmatrix} J' & 1 & J \\ M' & -q & -M \end{pmatrix} \left. \right] \\
&= (-1)^{m+m'-k'_1-k_2} \frac{(2J+1)(2J'+1)}{2} \left[\begin{pmatrix} J & 1 & J' \\ k_1 & 1 & -k'_1 \end{pmatrix} + \begin{pmatrix} J & 1 & J' \\ k_1 & -1 & -k'_1 \end{pmatrix} \right] \\
&\left[\begin{pmatrix} J' & 1 & J \\ k'_2 & -1 & -k_2 \end{pmatrix} + \begin{pmatrix} J' & 1 & J \\ k'_2 & 1 & -k_2 \end{pmatrix} \right] \sum_q (-1)^{q+1} \begin{pmatrix} J & 1 & J' \\ M & q & -M' \end{pmatrix} \begin{pmatrix} J' & 1 & J \\ M' & -q & -M \end{pmatrix}
\end{aligned}$$

Appendix B

Classical Motion of a QHO using Thermal Wavefunction

Beginning with our definition for time-dependent expectation value of our thermal wavefunction of a system (that is at thermal equilibrium), we may look at the time-dependent behaviour of a quantum-harmonic oscillator, and look at the conditions in order to obtain classical-like motion. In doing so, we see that the condition is for a 'coherent-like' state, although not a coherent-state in the strict sense as this definition of a wavefunction is not an eigenfunction of the annihilation operator, nor is the uncertainty of the position - momentum minimized.

$$\frac{1}{Z} \sum_n \sum_m e^{-\frac{\beta(E_n+E_m)}{2}} e^{i(\theta_n-\theta_m)} e^{\frac{i(E_n-E_m)t}{\hbar}} \langle n | \hat{O} | m \rangle \quad (\text{B.1})$$

where the energy basis is the quantum harmonic oscillator energy basis, thus:

$$E_n = \hbar\omega\left(n + \frac{1}{2}\right) \quad (\text{B.2})$$

if we are interested in the position of the QHO, we may replace the \hat{O} with $\hat{x} = \hat{a} + \hat{a}^\dagger$.

Our expression becomes:

$$\frac{1}{Z} \sum_n \sum_m e^{-\frac{\beta(E_n+E_m)}{2}} e^{i(\theta_n-\theta_m)} e^{\frac{i(E_n-E_m)t}{\hbar}} \langle n | \hat{a} | m \rangle \quad (\text{B.3})$$

$$+ \frac{1}{Z} \sum_n \sum_m e^{-\frac{\beta(E_n+E_m)}{2}} e^{i(\theta_n-\theta_m)} e^{\frac{i(E_n-E_m)t}{\hbar}} \langle n | \hat{a}^\dagger | m \rangle \quad (\text{B.4})$$

$$(\text{B.5})$$

Since:

$$\hat{a} | m \rangle = \sqrt{m} | m - 1 \rangle \quad (\text{B.6})$$

and

$$\hat{a}^\dagger | m \rangle = \sqrt{m+1} | m + 1 \rangle \quad (\text{B.7})$$

we may evaluate the above expressions as:

$$\begin{aligned} & \frac{1}{Z} \sum_n \sum_m e^{-\frac{\beta(E_n+E_m)}{2}} e^{i(\theta_n-\theta_m)} e^{\frac{i(E_n-E_m)t}{\hbar}} \langle n | \hat{a} | m \rangle + H.C. \\ &= \frac{1}{Z} \sum_n \sum_m e^{-\frac{\beta(E_n+E_m)}{2}} e^{i(\theta_n-\theta_m)} e^{\frac{i(E_n-E_m)t}{\hbar}} \sqrt{m} \langle n | m - 1 \rangle + H.C. \end{aligned}$$

thus, $n = m-1$ or $m = n + 1$. making this substitution we find:

$$\begin{aligned}
& \frac{1}{Z} \sum_n \sum_m e^{-\frac{\beta(E_n+E_m)}{2}} e^{i(\theta_n-\theta_m)} e^{\frac{i(E_n-E_m)t}{\hbar}} \sqrt{m} \langle n|m-1 \rangle + H.C. \\
&= \frac{1}{Z} \sum_n e^{-\frac{\beta(E_n+E_{n+1})}{2}} e^{i(\theta_n-\theta_{n+1})} e^{\frac{i(E_n-E_{n+1})t}{\hbar}} \sqrt{n+1} + H.C.
\end{aligned}$$

noting that:

$$E_n - E_{n+1} = \hbar\omega\left(n + \frac{1}{2}\right) - \bar{\omega}\left(n + 1 + \frac{1}{2}\right) = \hbar\omega \quad (\text{B.8})$$

and that:

$$E_n + E_{n+1} = \hbar\omega\left(n + \frac{1}{2}\right) + \bar{\omega}\left(n + 1 + \frac{1}{2}\right) = 2\hbar\omega(n+1) \quad (\text{B.9})$$

we can further simplify this to:

$$\begin{aligned}
& \frac{1}{Z} \sum_n e^{-\frac{\beta(E_n+E_{n+1})}{2}} e^{i(\theta_n-\theta_{n+1})} e^{\frac{i(E_n-E_{n+1})t}{\hbar}} \sqrt{n+1} + H.C. \\
&= \frac{e^{-\beta\hbar\omega}}{Z} \sum_n e^{-\beta\hbar\omega n} e^{i(\theta_n-\theta_{n+1})} e^{i\omega t} \sqrt{n+1} + H.C.
\end{aligned}$$

rewriting $\theta_n - \theta_{n+1}$ as just $\Delta\theta_n$, we find

$$\frac{e^{-\beta\hbar\omega}}{Z} \sum_n e^{-\beta\hbar\omega n} e^{i\Delta\theta_n} e^{i\omega t} \sqrt{n+1} + H.C. \quad (\text{B.10})$$

after grouping the complex exponentials together:

$$\frac{e^{-\beta\hbar\omega}}{Z} \sum_n e^{-\beta\hbar\omega n} e^{i(\Delta\theta_n + \omega t)} \sqrt{n+1} + H.C. \quad (\text{B.11})$$

Since we are adding the H.C., this is the same as taking 2xRe of the expression, and we have:

$$\frac{2e^{-\beta\hbar\omega}}{Z} \text{RE} \left[\sum_n e^{-\beta\hbar\omega n} e^{i(\Delta\theta_n + \omega t)} \sqrt{n+1} \right] \quad (\text{B.12})$$

which is equivalent to:

$$\frac{2e^{-\beta\hbar\omega}}{Z} \sum_n \sqrt{n+1} e^{-\beta\hbar\omega n} \cos(\Delta\theta_n + \omega t) \quad (\text{B.13})$$

Thus, in order to have a classical-like motion of the QHO in a system defined by thermal wavefunction, we require that the difference in phase of each $n, n+1$ state to be either 0, or a constant. If the difference is a constant, this is really the same as originally having the $\theta_n = \theta_{n+1} = \theta_{n+2} = 0$, and then propogating this 'coherent' state in time using the time-propagator.

If we set this condition, our final expression becomes:

$$\frac{2e^{-\beta\hbar\omega}}{Z} \sum_n \sqrt{n+1} e^{-\beta\hbar\omega n} \cos(\omega t) \quad (\text{B.14})$$

This can be seen as a frozen wave-packet whose expectation value oscillates back and forth in time, the magnitude of these oscillations equivalent to some thermodynamic average. This is similar to a 'coherent' state in the sense that in order to achieve this classical type motion, the energy associated to each eigen state must be 'in phase' or 'coherent'.

It can be noted that the thermal wavefunctions may be turned into a coherent-state in the strict sense if we instead define the overlap of the wavefunction with the energy eigenbasis as:

$$\begin{aligned} |\psi(\beta)\rangle &= \sum_n |n\rangle \langle n|\psi(\beta)\rangle \\ &= \frac{1}{\sqrt{Z}} \sum_n \frac{e^{-\frac{\beta E_n}{2}} e^{i\theta_n}}{\sqrt{n!}} |n\rangle \end{aligned}$$

which just changes the distribution of eigenstates from a Boltzmann distribution to a Poisson distribution.

Appendix C

Useful Snippets of Code

All of the code shown here is written in the python language.

C.1 Little-D Function

The following 'littleD' function can be called with the arguments of J,m,mp, and theta, in order to return the proper small-d rotation matrix.

```
def littleD(ldJ,ldmp,ldm,ldtheta):
    dval = np.sqrt(np.math.factorial(ldJ+ldm)*np.math.factorial(ldJ-ldmp)*np.math.factorial(ldJ+ldmp)*np.math.factorial(ldJ-ldmp))
    tempD = 0.

    #determine max v that will begin to give negative factorial arguments
    if ldJ - ldmp > ldJ + ldm:
        upper = ldJ-ldmp
    else:
        upper = ldJ+ldm

    #iterate over intergers that provide non-negative factorial arguments
    for v in range(upper+1):
        a = ldJ - ldmp - v
        b = ldJ + ldm - v
        c = v + ldmp - ldm
        if (a>=0) and (b>=0) and (c>=0):
            tempD = tempD + (((-1.0)**v)/(np.math.factorial(a)*np.math.factorial(b)*np.math.factorial(c)*np.math.factorial(v)))*((np.cos(ldtheta/2.))**(2.*ldJ+ldm-ldmp-2.*v))*((-np.sin(ldtheta/2.))**(ldmp-ldm+2.*v))
    return dval*tempD
```

C.2 Rotational Hamiltonian Setup

The following algorithm sets up an asymmetric top rotational Hamiltonian in the symmetric top basis using the matrix elements derived previously. Here, jkm is the basis size of the JKM basis up to a predefined Jmax.

```

#return off-diagonal matrix element
def off_diag (j,k):
    f = np.sqrt((j*(j+1)) - (k*(k+1)))
    return f

#####
#calculate Hrot#
#####
Hrot = np.zeros((jkm,jkm),dtype=float)
Jpos = 0
for J in range(Jmax+1):
    Jppos = 0
    for Jp in range(Jmax+1):
        for M in range(-J,J+1):
            for Mp in range(-Jp,Jp+1):
                for K in range(-J,J+1):
                    for Kp in range(-Jp,Jp+1):
                        if delta(J,Jp) == 1 and delta(M,Mp) ==1:
                            if delta(K,Kp-2)==1:
                                Hrot[Jpos + (K+J)*(2*J+1) + (M+J)][ Jppos + (Kp+Jp)*(2*Jp+1) + (Mp+Jp)] += 0.25*(Ah2o-Ch2o)
*off_diag(J,K)*off_diag(J,K+1)
                            if delta(K,Kp+2)==1:
                                Hrot[Jpos + (K+J)*(2*J+1) + (M+J)][ Jppos + (Kp+Jp)*(2*Jp+1) + (Mp+Jp)] += 0.25*(Ah2o-Ch2o)
*off_diag(J,K-1)*off_diag(J,K-2)
                            if delta(K,Kp)==1:
                                Hrot[Jpos + (K+J)*(2*J+1) + (M+J)][ Jppos + (Kp+Jp)*(2*Jp+1) + (Mp+Jp)] += (0.5*(Ah2o + Ch2o)*(J*(J+1)) + (Bh2o - 0.5*(Ah2o+Ch2o))*(K**2))
                                Jppos += (2*Jp+1)**2
                                Jpos+=(2*J+1)**2

```

C.3 Indexing and Basis Size Formulas

In order to calculate the total basis size of the JKM basis given a Jmax and including all of the K and M quantum numbers, the basis size can be calculated as:

$$\text{size} = ((2*J_{\text{max}} + 1) * (2*J_{\text{max}} + 2) * (2*J_{\text{max}} + 3)) / 6$$

Likewise for the nlm basis, given an nmax, we may determine the size as:

$$\text{size} = ((N_{\text{max}} + 1) * (N_{\text{max}} + 2) * (N_{\text{max}} + 3)) / 6$$

While iterating through the JKM basis, the position can be kept track using the following index formula:

$$\text{jpos} = (2 * (J-1) + 1) * (2 * (J-1) + 2) * (2 * (J-1) + 3) / 6 + (K+J) * (2*J+1) + (M+J)$$

Which, when iterated through $J=0$ to J_{\max} , will count from 0 to the max basis size (1, 2, 3, 4,... basis size)